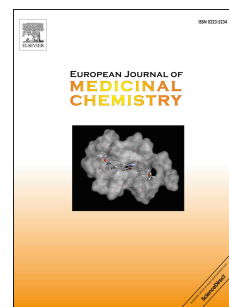# Accepted Manuscript

Discovery of new azoles with potent activity against *Candida* spp. and *Candida albicans* biofilms through virtual screening

Suat Sari, Didem Kart, Naile Öztürk, F. Betül Kaynak, Melis Gencel, Gülce Taşkor, Arzu Karakurt, Selma Saraç, Şebnem Eşsiz, Sevim Dalkara

MIC
C. albicans: 0.125 µg/ml
C. krusei: 0.5 µg/ml
C. parapsilosis: 0.25 µg/ml
C. tropicalis (resistant): 1 µg/ml

Anti-biofilm (*C. albicans*)
MBIC: 2 µg/ml
MBEC: 128 µg/ml

Discovery of new azoles with potent activity against *Candida* spp. and *Candida albicans* biofilms through virtual screening

Suat Sari[a]*, Didem Kart[b], Naile Öztürk[c,d], F. Betül Kaynak[e], Melis Gencel[f], Gülce Taşkor[g], Arzu Karakurt[h], Selma Saraç[a], Şebnem Eşsiz[e], Sevim Dalkara[a]

[a] Hacettepe University, Faculty of Pharmacy, Department of Pharmaceutical Chemistry, 06100, Ankara, Turkey

[b] Hacettepe University, Faculty of Pharmacy, Department of Pharmaceutical Microbiology, 06100, Ankara, Turkey

[c] Hacettepe University, Faculty of Pharmacy, Department of Pharmaceutical Technology, 06100, Ankara, Turkey

[d] İnönü University, Faculty of Pharmacy, Department of Pharmaceutical Technology, 44280, Malatya, Turkey (permanent address)

[e] Hacettepe University, Faculty of Engineering, Department of Physical Engineering, 06800, Ankara, Turkey

[f] Kadir Has University, Faculty of Engineering and Natural Sciences, Department of Bioinformatics and Genetics, 34083, Istanbul, Turkey

[g] Hacettepe University, Faculty of Pharmacy, Department of Basic Pharmaceutical Sciences, 06100, Ankara, Turkey

[h] İnönü University, Faculty of Pharmacy, Department of Pharmaceutical Chemistry, 44280, Malatya, Turkey

Declarations of interest: none

* Correspondence: Suat Sari, PhD
Hacettepe University Faculty of Pharmacy
Department of Pharmaceutical Chemistry
06100 Sihhiye Ankara/TURKEY
Tel.: + 90 312 305 18 72
Fax: + 90 312 305 32 72
e-mail: suat.sari@hacettepe.edu.tr
   suat1039@gmail.com

Abstract

Systemic candidiasis is a rampant bloodstream infection of *Candida* spp. and *C. albicans* is the major pathogen isolated from infected humans. Azoles, the most common class of antifungals which suffer from increasing resistance, and especially intrinsically resistant non-*albicans Candida* (NAC) species, act by inhibiting fungal lanosterol 14α-demethylase (CYP51). In this study we identified a number of azole compounds in 1-(2,4-dichlorophenyl)-2-(1*H*-imidazol-1-yl)ethanol/ethanone oxime ester structure through virtual screening using consensus scoring approach, synthesized and tested them for their antifungal properties. We reached several hits with potent activity against azole-susceptible and azole-resistant *Candida* spp. as well as biofilms of *C. albicans*. **5i**'s minimum inhibitor concentration (MIC) was 0.125 µg/ml against *C. albicans*, 0.5 µg/ml against *C. krusei* and 1 µg/ml against azole-resistant *C. tropicalis* isolate. Considering the MIC values of fluconazole against these fungi (0.5, 32 and 512 µg/ml, respectively), **5i** emerged as a highly potent derivative. The minimum biofilm inhibitor concentration (MBIC) of **5c**, **5j**, and **5p** were 0.5 µg/ml (and **5i** was 2 µg/ml) against *C. albicans* biofilms, lower than that of amphotericin B (4 µg/ml), a first-line antifungal with antibiofilm activity. In addition, the active compounds showed neglectable toxicity to human monocytic cell line. We further analyzed the docking poses of the active compounds in *C. albicans* CYP51 (CACYP51) homology model catalytic site and identified molecular interactions in agreement with those of known azoles with fungal CYP51s and mutagenesis studies of CACYP51. We observed the stability of CACYP51 in complex with **5i** in molecular dynamics simulations.

Keywords: consensus scoring; azoles; *Candida albicans*; biofilm; cytotoxicity; molecular docking; molecular dynamics simulations

1. Introduction

Systemic candidiasis is a major public health issue, especially with immune-suppressed cases reaching high mortality rates. The members of the genus *Candida* are the most frequently recovered from human fungal infection and *Candida albicans*, so far, is the leading pathogen identified in nosocomial candidiasis [1]. In addition to increasing drug-resistant strains of *C. albicans*, emergence of non-*albicans Candida* spp. (NAC) complicate the treatment of mycoses [2]. *C. tropicalis* is among the NACs that show reduced susceptibility to first-line antifungals reportedly leading to breakthrough fungemia among high-risk patients [3, 4]. Also, *C. krusei* is known to be intrinsically resistant to a number of azoles including fluconazole [5]. One of the several mechanisms of therapy-resistance is formation of biofilms, which are complex microorganism colonies enclosed in an exopolysaccharide matrix on biotic and non-biotic surfaces. Persistent biofilms make fungi much less susceptible to antifungal drugs compared to their planktonic forms for a number of reasons [6-8]. Therefore it is essential to design new molecules effective against resistant fungi as well as fungal biofilms.

Azoles are commonly preferred in fungal infections for their advantages such as broad spectrum of activity, well-tolerability, and oral availability (Fig. 1), however their wide usage brings about the issue of resistance [9]. Azoles act through inhibition of lanosterol 14α-demethylase (CYP51), a ubiquitous cytochrome P450 enzyme that plays a key role in the biological synthetic cascade of ergosterol, a fungal sterol included in membrane structure [10]. The emergence of experimental fungal CYP51 structures accelerated the efforts towards rational design of new azoles [11-16]. Also merging molecular modelling studies with mutational studies lead to identification of key molecular determinants for CYP51 inhibition to better design new hits [11, 12, 17].
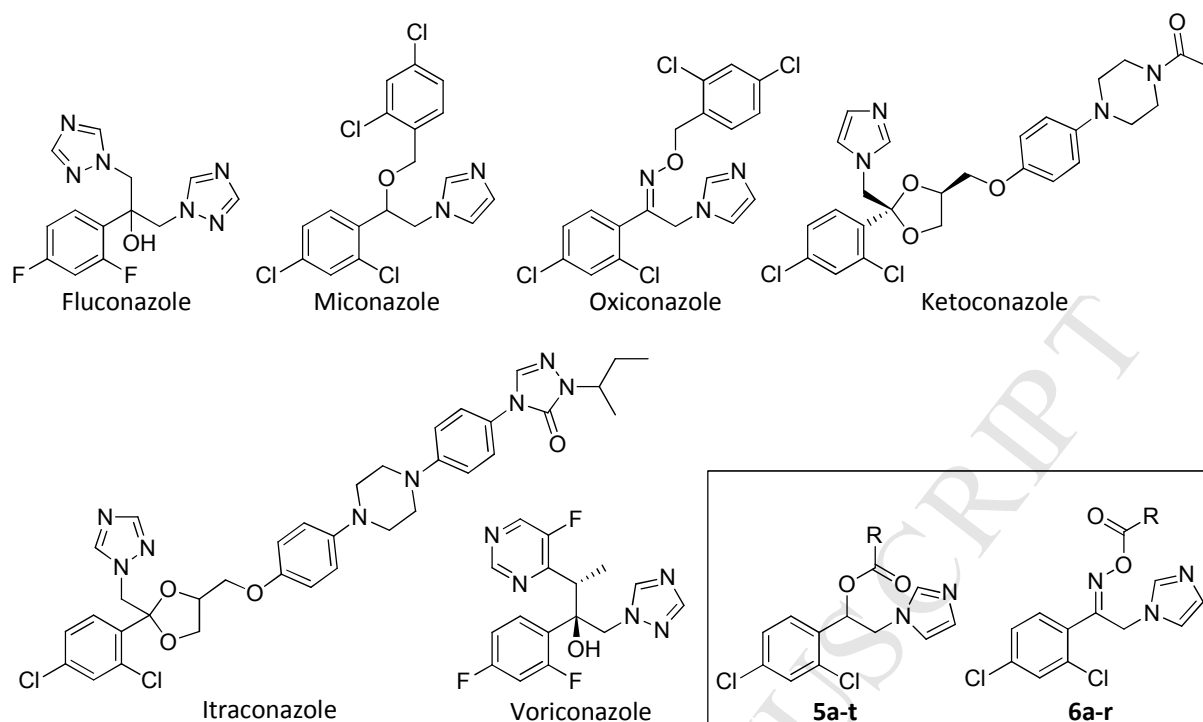
Fig. 1. Molecular structure of azole antifungals from different generations and the title compounds

In this study we present rational design of a set of miconazole and oxiconazole analogues (**5a-t** and **6a-r**) through virtual screening, their synthesis and biological activity studies (Fig. 1). We obtained hit molecules with activity against azole-resistant *C. tropicalis* as well as inhibition of *C. albicans* biofilms. The active compounds showed neglectable cytotoxicity. Also, in-depth analysis of *C. albicans* CYP51 (CACYP51) inhibition via molecular modelling studies provided valuable insights.

2. Results and discussion

2.1. Identification of the compounds for synthesis through virtual screening

2.1.1. Virtual library generation and physicochemical properties filtering

Azole antifungals feature a number of pharmacophores: an azole group, an aromatic ring, and a "tail" group attached to an alkylene bridge between the two via various linker groups. In our study, we constructed an azole scaffold with imidazole as the azole ring, 2,4-dichlorophenyl as the aromatic ring, either alcohol ester or oxime ester as the linker functionalities for the tail defined as R in Fig. 1. We, then, envisaged a virtual library of more than 200 compounds by modifying the tail considering the commercially available synthetic building blocks, i.e. carboxylic acids, for this position. The virtual library was created by 3D-modelling the envisaged compounds with proper tautomeric and ionization forms and

enantiomers, and geometry optimization, and subjected to a drug-likeness filtering to eliminate the candidates with poor physicochemical properties such as molecular weight (MW), number of rotatable bonds (RB), hydrogen bond donor and acceptor counts (HD and HA), octanol/water partition coefficient (LogP), and total polar surface area (PSA) [18-20]. Compounds with more than two "Lipinski's rule of 5" violations were phased out and the remaining 146 compounds were selected for the next step.

2.1.2. Molecular docking and consensus scoring

The eukaryotic CYP51 is composed of a catalytic domain which contains a heme co-factor at the bottom of the catalytic site. An anchor domain attached to the catalytic domain tethers the enzyme to endoplasmic reticulum (ER) membrane. A narrow, hydrophobic entry channel, reaching from a location close to where the two domains connect and the ER membrane, leads to the catalytic cavity and heme. According to the crystallographic data azoles occupy this catalytic domain with a common conformation in the following way: the azole group interacts with the heme making the 6th axial coordination with heme iron through one of the nitrogen atoms, the aromatic ring fits in a cavity between the heme and the protein in hydrophobic contacts and the tail, which includes H bond donors and acceptors in addition to hydrophobic groups, occupies the entry channel (Fig. 2) [21, 22].

<Figure 2>

Fig. 2. The catalytic site of *Saccharomyces cerevisiae* CYP51 (protein is showed as rippons and the binding site molecular surface is rendered) with the co-crystallized ligand itraconazole (green sticks) interacting with heme cofactor (gray sticks) and heme iron (orange sphere).

Although the azole ring-heme interaction is key to this binding, the interactions of the tail with this gorge determine the tightness of this binding [23]. In this respect we docked the remaining 146 compounds from the previous step to the catalytic site of CACYP51 homology model using AutoDock (v4.2) [24] and Glide (2018-1: Schrödinger, LLC, NY, 2018) [25-27]. We determined the docking scores of each compound from the two software out of the best poses identified upon visual inspection in comparison with the available crystallographic data. The compounds were then ranked as two separate groups, alcohol ester and oxime ester derivatives, according to their consensus scores, which, simply, is the average of the

scores from AutoDock and Glide (See Table S1 of Supporting Information for the structures of the docked compounds and full results of the virtual screening study). Consensus scoring, which combines multiple scoring functions in binding affinity estimation, reportedly leads to higher hit-rates in virtual library screening studies by eliminating false positives since different scoring functions may bias certain interaction terms [28, 29]. Since AutoDock and Glide yield docking scores of compatible units we preferred the rank-by-number strategy, in which we simply ranked the compounds according to the mean values of the scores from each. Other strategies are rank-by-rank, in which the compounds are ranked by their mean rank values obtained from each scoring function instead of docking score, and the rank-by-vote strategy, in which the compounds are assigned a number for each scoring function according to the percentage they are ranked in each scoring function and then ranked according to the mean value of these numbers [28]. Compounds with top consensus score among the two groups were selected for synthesis (Table 1). Some of the top-scoring compounds were skipped in the synthesis step due to no or very low yield through the common synthetic protocol described below (see Table S1 of Supporting Information for details).

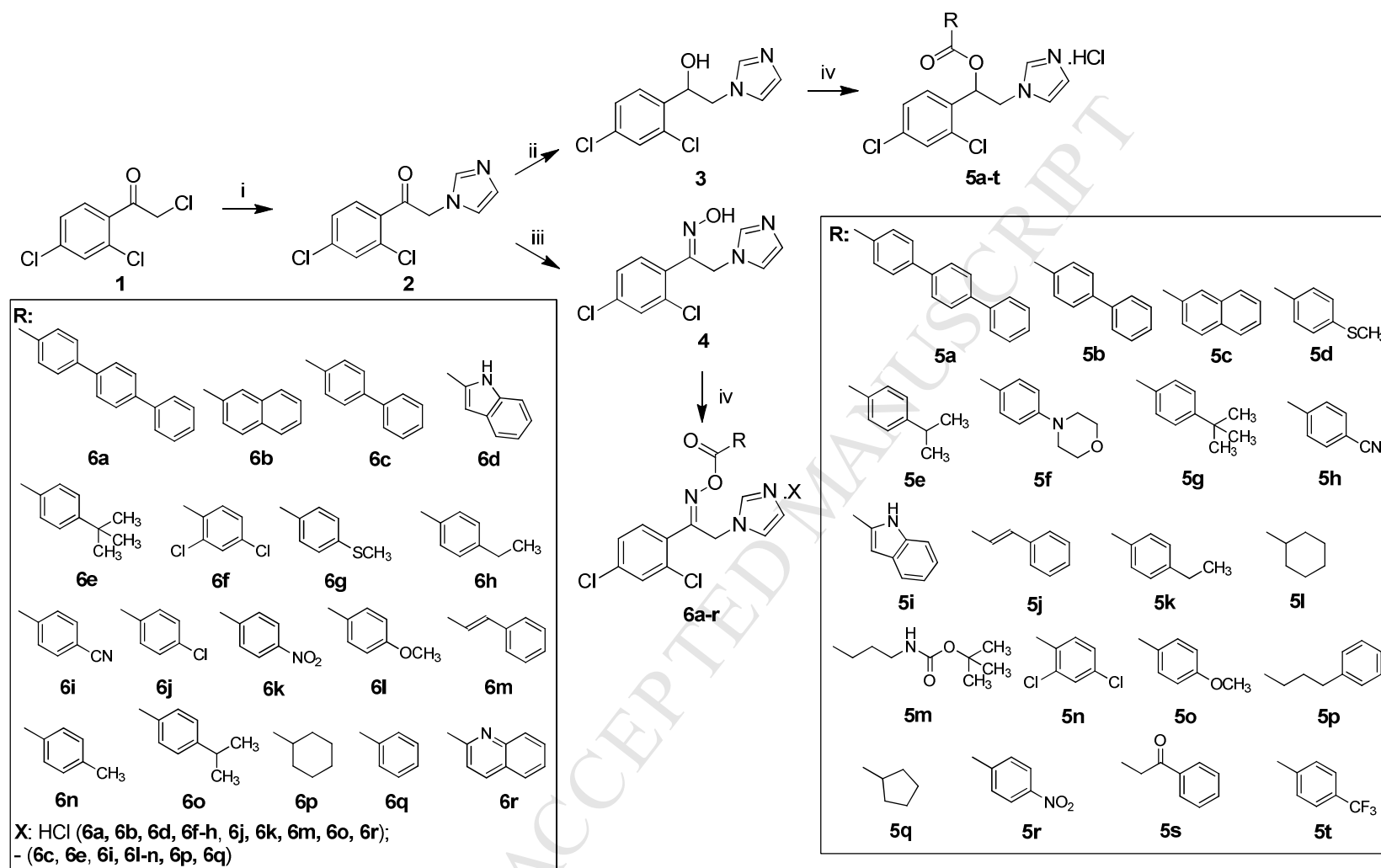**Table 1**. Virtual screening scores (kcal/mol) of the selected compounds.

Comp.	AutoDock	Glide	consensus[a]	Comp.	AutoDock	Glide	consensus[a]
5a	-11.79	-5.40	-8.60	6a	-12.56	-5.77	-9.17
5b	-10.48	-6.34	-8.41	6b	-10.14	-6.59	-8.37
5c	-9.41	-6.42	-7.92	6c	-10.5	-5.84	-8.17
5d	-8.36	-6.91	-7.64	6d	-8.87	-6.98	-7.93
5e	-8.99	-6.23	-7.61	6e	-9.68	-6.01	-7.85
5f	-9.09	-6.11	-7.60	6f	-8.97	-6.14	-7.56
5g	-9.27	-5.89	-7.58	6g	-8.63	-6.46	-7.55
5h	-8.14	-6.78	-7.46	6h	-8.70	-6.33	-7.52
5i	-8.24	-6.65	-7.45	6i	-8.63	-6.34	-7.49
5j	-8.85	-6.03	-7.44	6j	-8.69	-6.19	-7.44
5k	-8.63	-5.84	-7.24	6k	-8.53	-6.27	-7.40
5l	-8.35	-6.08	-7.22	6l	-8.64	-6.06	-7.35
5m	-8.24	-6.06	-7.15	6m	-9.04	-5.39	-7.22
5n	-8.15	-6.08	-7.12	6n	-8.55	-5.88	-7.22
5o	-8.06	-6.16	-7.11	6o	-9.12	-5.26	-7.19
5p	-8.28	-5.88	-7.08	6p	-8.58	-5.62	-7.10
5q	-7.97	-6.11	-7.04	6q	-8.26	-5.77	-7.02
5r	-8.10	-5.63	-6.87	6r	-7.94	-6.05	-6.00
5s	-8.13	-5.44	-6.79				
5t	-8.11	-5.42	-6.77				

2.2. Synthesis of the selected compounds

The synthetic procedure for the selected compounds is outlined in Scheme 1. Synthesis of **5g**, **5j**, **5n**, and **5r** was previously reported [30, 31]. Starting from 2,2',4'-trichloroacetophenone (**1**) we obtained 1-(2,4-dichlorophenyl)-2-(1*H*-imidazol-1-yl)ethanone (**2**) by *N*-alkylation of imidazole with **1** in dimethylformamide (DMF). **2** was reduced using sodium borohydride ($NaBH_4$) methanol (MeOH) to yield 1-(2,4-dichlorophenyl)-2-(1*H*-imidazol-1-yl)ethanol (**3**) and converted to its oxime derivative 1-(2,4-dichlorophenyl)-2-(1*H*-imidazol-1-yl)ethanone oxime (**4**) using first hydroxylamine hydrochloride ($NH_2OH.HCl$) at basic medium and refluxing in ethanol (EtOH) then at basic medium in water. The title compounds (**5a-t** and **6a-r**) were afforded through esterification of **3** and **4** with proper carboxylic acids in the presence of 4-dimethylaminopyridine (DMAP), a transacylation catalyst, and *N,N'*-dicyclohexylcarbodiimide (DCC), a coupling agent, in dry dichloromethane (DCM). **2**, **3**, **5b-t**, **6a**, **6b**, **6d**, **6f-h**, **6j**, **6k**, **6m**, **6o**, and **6r** were converted to their HCl salts using gaseous HCl (gHCl) to improve purity and solubility. Structures and purity of the compounds were confirmed via LC-MS and NMR spectra and elemental analysis.

Scheme 1. Synthesis of the selected compounds. Reagents and conditions: imidazole, DMF, 0-5 °C (i); NaBH$_4$, MeOH, 0-5 °C (ii); NH$_2$OH.HCl, EtOH, pH 14, ref., conc. HCl, H$_2$O, pH 5 (iii); RCOOH, DCC, DMAP, DCM, 0-5 °C, gHCl.

The HPLC chromatograms of the compounds showed a pure single peak whose mass spectrum included molecular ion peaks with $[M+2]^+$ and $[M+4]^+$ chlorine isotopes and their sodium adduct peaks. ^{1}H NMR spectra of the alcohol ester derivatives featured a multiplet between 4.5-5.0 ppm for the protons of CH_2 next to imidazole and a doublet of doublet at around 6.5 ppm for the CH proton of the alcohol root, which gave a multiplet signal for some compounds. The CH_2 next to the imidazole of the oxime ester derivatives was observed as a singlet around 6 ppm. The protons of 2,4-dichlorophenyl ring were observed in the aromatic region of the spectrum, usually overlapped with other aromatic protons of the tail groups as well as with H^4 and H^5 of the imidazole. Imidazole's H^2 resonated further downfield than H^4 and H^5 and the deshielding effect of the HCl salt was very obvious for this proton which resonated much further downfield, at around 9.2 ppm, compared to that of the derivatives without HCl observed at 8.1-8.4 ppm range. The protons of the tail groups were observed at chemical shifts corresponding to the functional groups they belong and the integration values of the signals were proportionate to the number of protons they represent. The ^{13}C NMR spectra were also in agreement with the structural composition of the compounds. The carbonyl carbons of the alcohol ester and oxime ester functions were observed at 160-164 ppm range and the oxime C=N-O carbon of the oxime ester resonated around 160 ppm (See Supporting Information for details).

2.3. X ray crystallography studies

According to the ORTEP [32] views, **4** is in *Z* configuration (Fig. 3), which is in accordance with our previous studies with oximes and their derivatives [33-35]. This finding supports the possibility that the title compounds in oxime ester derivatives are in the configuration, too. The packing of **4** is composed of *Z* isomers only, showing that **4** was obtained as *Z* isomer (Fig. 4). Molecular structure of **5o** was resolved as *R* enantiomer. In the crystal pack, however, consecutively aligned *R* and *S* isomers of 5o interact with each other through non-classical H bonds as expected since **5a-t** were synthesized as racemates through nonselective method. In both compounds, the 2,4-dichlorobenzene and imidazole rings are separately planar. The 2,4-dichlorobenzene and imidazole rings of **5o** are almost in the same plane and the deviation from the planarity is 2.12°. The dihedral angles between the imidazole ring and the 4-methoxybenzene ring and the 2,4-dichlorobenzene ring of **5o** are 77.16° and 75.60°, respectively. For **4**, the dihedral angle between 2,4-dichlorobenzene and imidazole rings is

54.38°. The crystal structures **4** and **5o** are stabilized by intermolecular and intramolecular hydrogen bonds. There are also C–C*l*…π interactions in their crystal structures. For more details see Table S3 and Table S4 of Supporting Information.

<Figure 3>

Fig. 3. ORTEP3 view of **4** (A) and **5o** (B) showing the atom-numbering scheme. Displacement ellipsoids are drawn at 50% (A) and 35% (B) probability level.

<Figure 4>

Fig. 4. Hydrogen bonding interactions of **4** (A) and **5o** (B), the unit cell packing of **4** (C, view direction is along [100]), and **5o** (D, view direction is along [010]).

2.4. *Candidae* susceptibility to the synthesized compounds

We identified the minimum inhibitor concentration (MIC) values of the synthesized compounds against the ATCC strains of *C. albicans*, *C. parapsilosis*, and *C. krusei*. Some of the active compounds were also tested against an azole-resistant clinical isolate of *C. tropicalis* (Table 2). MIC is the minimum concentration of material that inhibits visual growth of a given microorganism. Many compounds were found active against *C. albicans* at concentrations better than or comparable to fluconazole. Especially, **5b**, **5i**, **5j**, and **6l** stood out as derivatives with MIC values better than or equal to fluconazole. Several compounds were also active against *C. krusei*, a NAC known to be resistant against many azoles, at very low MICs. **5c**, **5i**, **5j**, and **5o** were found highly potent against the azole-resistant *C. tropicalis* isolate. MIC values of **5g**, **5j**, **5n**, and **5r** against *C. albicans* were previously reported as 10, 2, 300, and >300 μg/ml, respectively [30, 31]. The efficacy of **5j** was thus confirmed.

Table 2. MIC values (μg/ml) of the compounds against *Candida* spp.

Compound	*C. albicans* ATCC 90028	*C. krusei* ATCC 6258	*C. parapsilosis* ATCC 90018	*C. tropicalis* isolate
2	128	256	32	
3	8	128	4	256
4	32	256	32	
5a	256	256	256	
5b	0.25	1	0.25	512
5c	1	2	1	1
5d	8	28	16	
5e	256	128	128	
5f	16	256	32	

5g	128	256	128	
5h	8	64	4	16
5i	0.125	0.5	0.25	1
5j	0.5	1	1	4
5k	256	256	256	
5l	8	32	4	16
5m	8	128	16	
5n	128	256	128	
5o	2	16	1	4
5p	2	8	2	32
5q	1	16	2	8
5r	8	32	4	8
5s	16	32	8	
5t	256	256	256	
6a	128	256	128	
6b	256	256	256	
6c	1	1	1	256
6d	128	256	128	256
6e	4	4	4	64
6f	64	64	64	
6g	2	64	2	16
6h	128	256	128	8
6i	128	64	64	
6j	32	64	32	
6k	64	64	16	
6l	0.5	1	1	64
6m	2	4	2	64
6n	128	256	256	
6o	16	32	16	
6p	64	64	64	
6q	32	32	32	
6r	128	256	256	
Fluconazole	0.5	32	0.5	512

Biofilm formation is one of the common drug resistance mechanisms of fungi. Among the most active derivatives, twelve were tested against mature biofilms of *C. albicans*, the minimum biofilm inhibitor and the minimum biofilm eradicator concentration (MBIC and MBEC) values were determined for each of the twelve compounds (Table 3). Most of the tested compounds (**5b**, **5c**, **5i**, **5j**, **5o**, **5p**, **6g**, and **6l**) better inhibited biofilm formation than amphotericin B, a first-line antifungal drug known for its efficacy against fungal biofilms. The MBIC of **5j** against *C. albicans* biofilms was reported as 2 µg/ml [31]. Biofilm eradicator potential of the compounds were low, like amphotericin B, however the MBEC values of **5j** and **5p** were promising.

**Table 3**. MBIC and MBEC values (µg/ml) of the selected compounds against *C. albicans* biofilms.

Compound	MBIC	MBEC
5b	2	256
5c	0.5	256
5i	2	128
5j	0.5	64
5o	1	256
5p	0.5	64
5q	32	>1024
6c	16	256
6e	128	256
6g	2	256
6l	2	512
6m	128	512
Amphotericin B	4	256

From the antifungal susceptibility assays, derivatives **5c**, **5i**, **5j**, and **5o** emerged as the most potent compounds with activity against ATCC strains of *C. albicans* and other NACS, against an azole-resistant *C. tropicalis* isolate, and *C. albicans* biofilms at the same time (Table 2 and Table 3). The alcohol ester library was apparently more active than the oxime ester library, which includes potent derivative such as **6c**, **6g**, **6l**, and **6m**. All these active derivatives bear a benzene ring on the tail. 4-Biphenyl, cinnamyl, indol-2-yl, 4-methoxyphenyl, and 2-naphthyl emerged as the most useful substitutions for the tail group. However the most potent compound against *C. albicans*, **5i**, is the only one with a hydrogen bond donor. The most potent derivatives against the *C. tropicalis* isolate was again the alcohol ester derivatives, **5c**, **5i**, **5j**, and **5o**, which bear 2-naphthyl, indol-2-yl, cinnamyl, and 4-methoxyphenyl, respectively. Interestingly, compounds with potent activity against the ATCC Candida strains such as **5b** and **6c**, which bear 4-biphenyl tail, were almost ineffective against this isolate.

2.5. Cytotoxicity evaluation

Selectivity of antimicrobial chemotherapeutic agents towards the microorganism and their safety to the host is crucial. For the *in vitro* cytotoxicity evaluation of the selected six active compounds (**5b**, **5c**, **5i**, **5j**, **6c,** and **6l**) cell viability of U937 human monocytic cells in the presence of the compounds after 24 and 48 hours were determined in comparison with the control (Fig. 5A and Fig. 5B). The compounds did not display considerable toxicity at their

active concentration ranges at any time points, although **5b** lowered the viability percentages below 80% at concentrations ≥ 8 μg/ml.
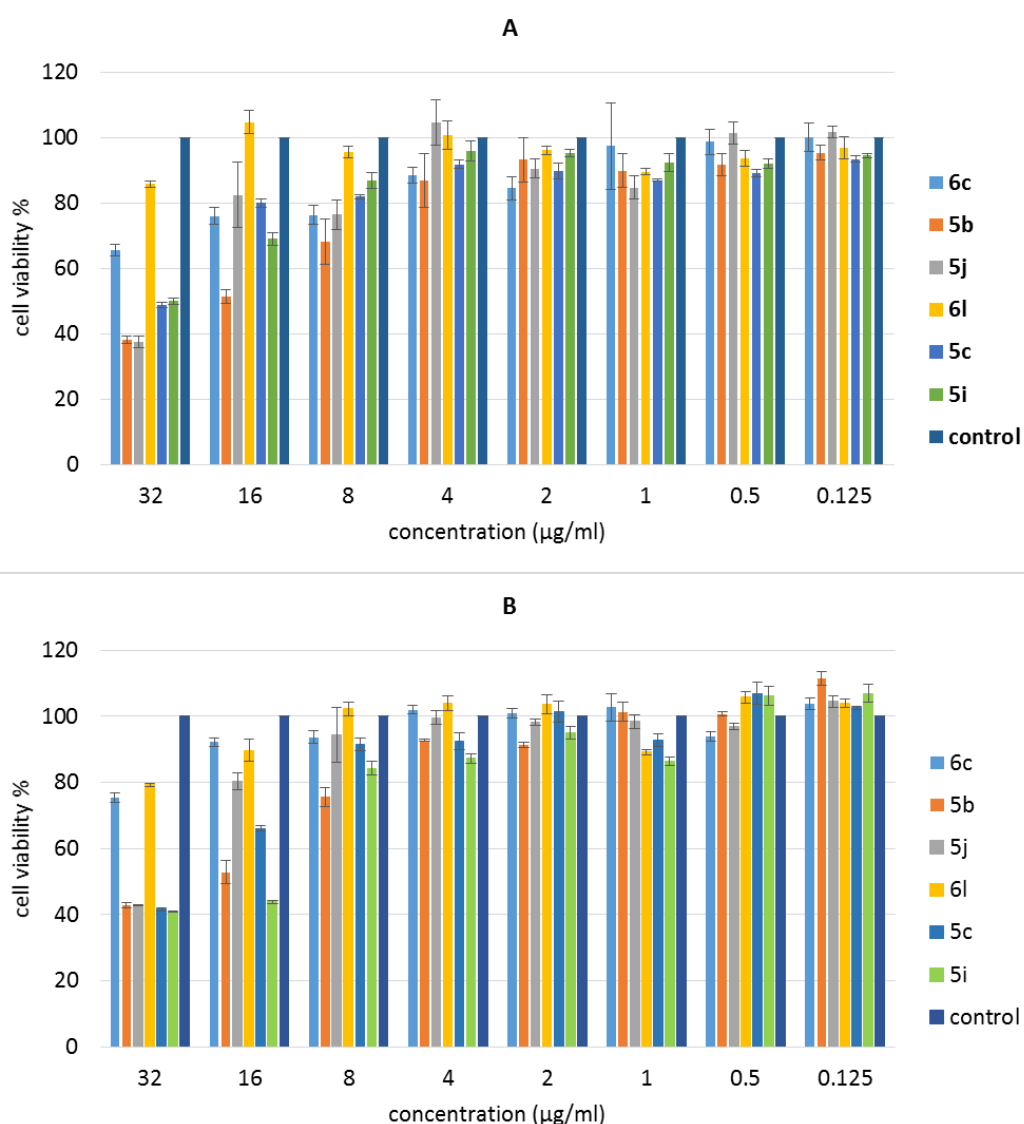
Fig. 5. The effect of **5b**, **5c**, **5i**, **5j**, **6c**, and **6l** on cell viability of human monocytic cell line for 24 h (A) and 48 h (B).

2.6. Drug-like chemical space evaluation

The calculated molecular descriptors of the title compounds, in general, were within the recommended ranges derived from the known drug-like chemical space, although there were exceptions. The number of rotatable bonds, molecular weight, hydrogen bond donor and acceptor counts, and polar surface area were found within the limit values. The calculated LogP of **5a** and **6a** were too high, their aqueous solubility was also below the ideal limit, which probably was the reason for these compounds to be inactive. These compounds

violated the Lipinski's rule of five for having molecular weight greater than 500 g/mol and Log P value higher than 5 (See Table S2 of Supporting Information for the full data of the calculated descriptors).

2.7. Molecular modelling of CACYP51 inhibition by the active compounds

The binding modes of the active compounds obtained from AutoDock and Glide fulfilled the molecular determinants identified for CYP51 inhibition by azoles as described above (Fig. 6). The imidazole ring of the compounds was in T-shaped π-π interaction with the heme while the nitrogen at the second position of imidazole was in axial coordination with the heme iron. The 2,4-dichlorophenyl group was in the hydrophobic pocket just above the heme surrounded by residues Phe126, Ile131, Tyr132, and Gly303, and the tail occupied the entry channel (See Supporting Information for details). **5i**'s NH of indole at the tail donates a hydrogen bond to Ser378 backbone oxygen in the binding mode from AutoDock, but to Met508 in the binding mode from Glide. The compound also engages in a π-π interaction with Tyr132 according to AutoDock. Other residues that contact with the tail are Tyr118, Leu121, Thr122, Pro230, Leu376, Ile379, Phe380, and Val509 in both binding modes. Most of these residues cited as key residues for the enzyme activity in mutagenesis studies and their mutants were reportedly associated with decreased susceptibility to azoles [36].

<Figure 6>

Fig. 6. Superimposition of the binding modes of **5i** from AutoDock (light green) and Glide (dark green) in CACYP51 catalytic site (A), and their 2D interaction diagrams (B and C, respectively). Ligands and heme are represented as sticks, heme iron as blue CPK, and protein surface is rendered in color according to the electrostatic potential.

We further evaluated the **5i**-CACYP51 complex in terms of dynamic evolution and stability using molecular dynamics (MD) simulations. We selected the binding mode form AutoDock for this purpose due to its suitability to the available crystal structures, especially considering the orientation of imidazole regarding the heme, the distance between heme iron and N^2, as well as the orientation of the 2,4-dichlorophenyl ring in the hydrophobic cleft. We compared the trajectories of water solvated **5i**-bound CACYP51 and the ligand free (apo) CACYP51 systems. The Cα atoms RMSD and total energy plots indicate higher stability for the **5i**-bound system (Fig. 7A and Fig. 7B). The RMS fluctuation (RMSF) values for the residues also

show that most of the residues fluctuated more in the apo form (Fig. 7C). Phe228, Pro230, Gly307, and Met508 were the most fluctuating binding site residues in the absence of **5i**.
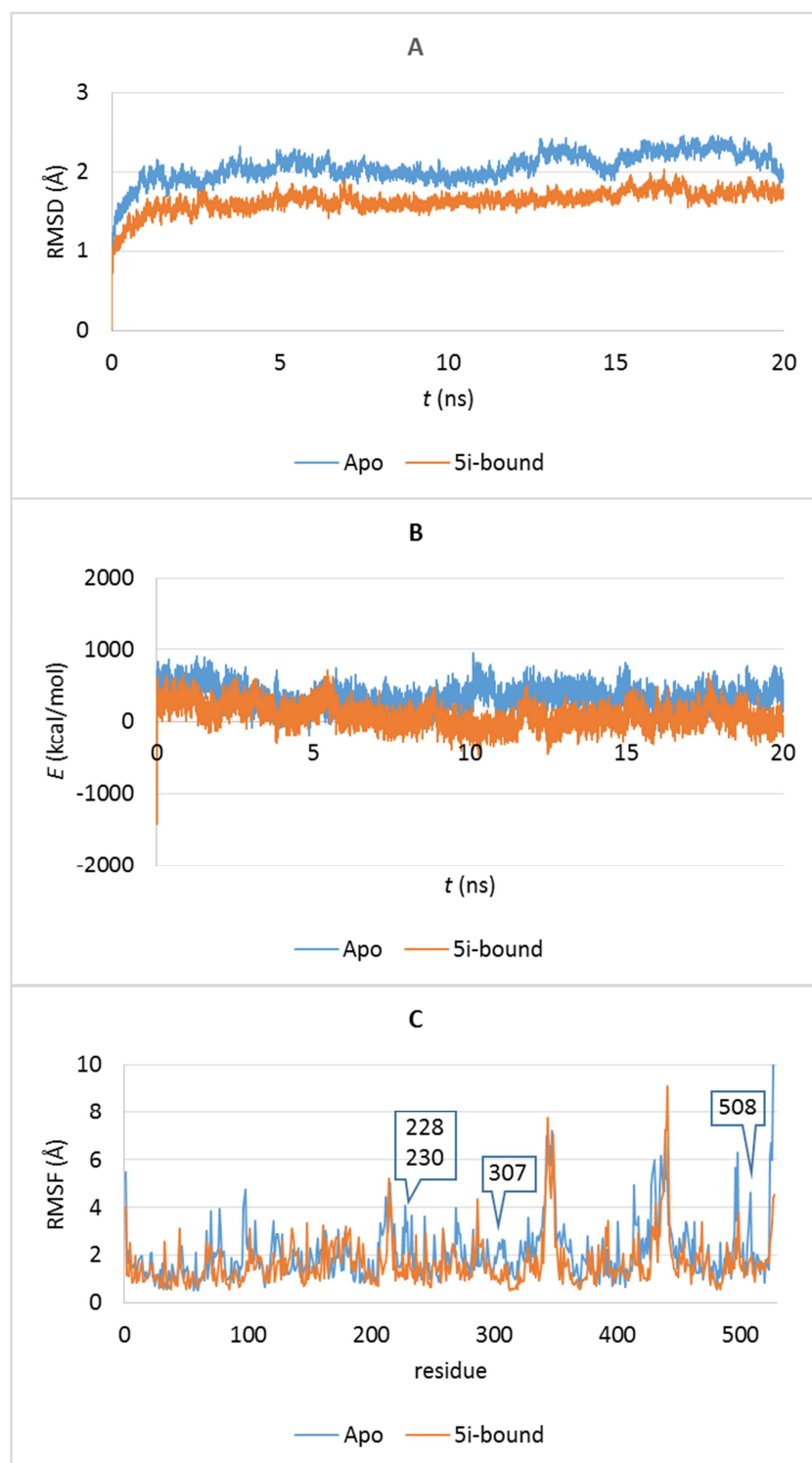
Fig. 7. Plots showing apo and **5i**-bound CACYP51's Cα RMSD values (A) and the total energy of the protein over time (B) and the average RMS fluctuations for each residue (C) (High fluctuating binding site residues are indicated).

We also monitored the hydrogen bond distance between the indole NH and Ser378 carbonyl oxygen as well as the distance between the 2,4-dichlorophenyl and Tyr132 side chain, which were in π-π stacks (Fig. 8). Both interactions maintained at around 4 Å although the hydrogen bond distance showed certain fluctuations.
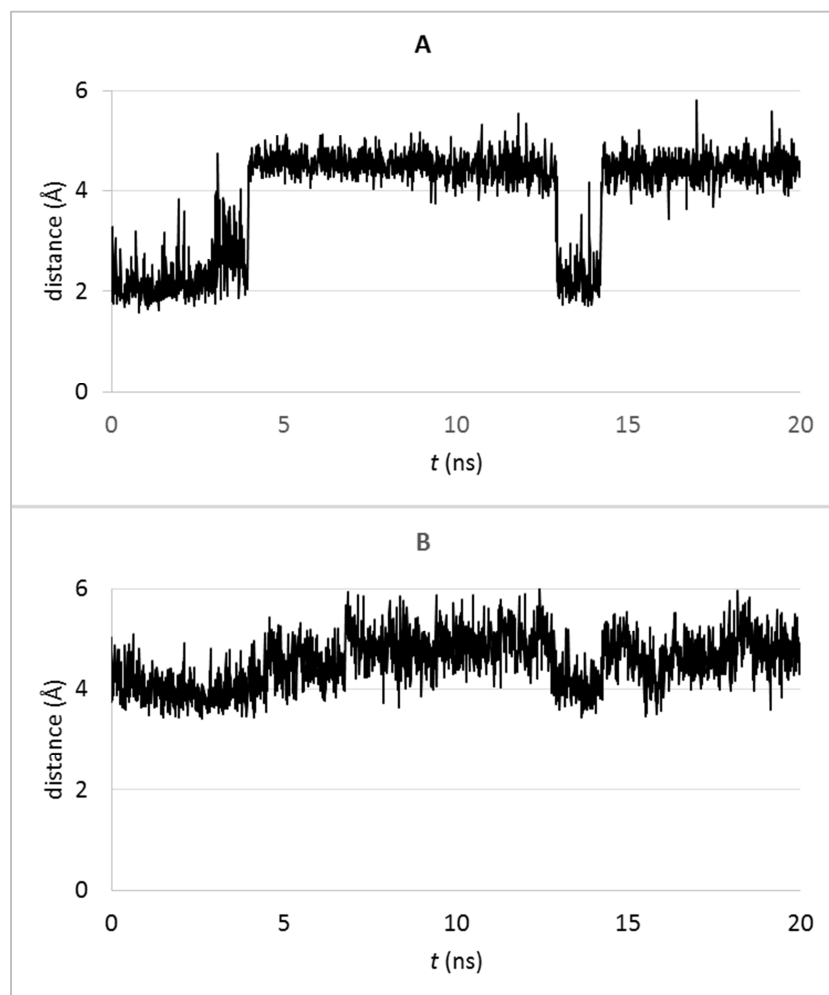
Fig. 8. Plots showing the deviation of the distance of the hydrogen bond between **5i**'s indole NH hydrogen and Ser378 (A) and the distance of the π-π interaction between **5i**'s 2,4-dichlorophenyl and Tyr132 side chain (B).

3.   Conclusion

In pursuit for ideally effective and safe antifungals in azole structure we took on a rational design study using virtual screening method and consensus scoring approach. The selected compounds were synthesized and tested against *Candida* spp. Fungi. We reached highly potent derivatives including **5i** with a MIC of 0.125 µg/ml against *C. albicans,* 0.5 µg/ml against *C. krusei*, 0.25 against *C. parapsilosis*, and 1 µg/ml against a fluconazole-resistant *C.*

tropicalis isolate. In addition **5b**, **5c**, **5i**, **5j**, **5o**, **5p**, **6g**, and **6l** were better at inhibiting *C. albicans* biofilms than amphotericin B, an antifungal drug with antibiofilm activity. Inhibiting fungal biofilms, which account for drug resistance of some fungi among other mechanisms and raises the inhibitor concentrations of first-line antifungals by orders compared to their MIC values against the planktonic forms, is a key feature of our compounds. Also, some of these compounds were tested and found safe for human monocytes at their active concentrations. Therefore, it is suggestable that our virtual screening study with rank-by-number consensus scoring strategy, which took advantage of two different scoring functions, paid off well with several hits and promising derivatives against drug-resistant fungi.

The binding modes and interactions of the active compounds from both AutoDock and Glide were in good agreement with the experimental and theoretical data. From the MD simulations we were able to deduce that CACYP51 was more stable with the presence of **5i** in its catalytic site with two key interactions, a hydrogen bond with Ser378 and π-π interaction with Tyr132 side chain.

This study yielded potent antifungal hits with excellent activity profile and future prospects for further optimization as leads due to favorable calculated descriptors putting them within the drug-like chemical space. With strong *in silico* evidence to their proposed mechanism of action we are now trying to design better CACYP51 inhibitors referring to the structure of **5i**.

4. Materials and Methods

4.1. Molecular modelling and virtual screening

The virtual library was created using 2D Sketcher and MacroModel (2018-1: Schrödinger, LLC, NY, 2018) of Maestro (2018-1: Schrödinger, LLC, NY, 2018). The ligands were then optimized using conjugate gradients method and OPLS_2005 force field [37]. Possible tautomeric and ionization states (pH: 7±2) and enantiomers for each ligand were modelled using LigPrep of Maestro. The molecular descriptors were calculated using QikProp (2018-1: Schrödinger, LLC, NY, 2018).

The homology modelling of CACYP51 was previously described [11]. In brief, it was created according to comparative modelling approach on MODELLER (v9.18) [38] using the pairwise amino acid sequence alignment of CACYP51 and *S. cerevisiae* CYP51 and the crystal structure

of the latter (PDB ID: 5EQB [21]) as template. The co-crystallized ligand, itraconazole in the active site of the template was included in the CACYP51 homology model. For grid generation the central coordinates of CACYP51 catalytic site (19.42 10.25 17.44) was selected and each dimension of the grid box was set to 20 Å. Each ligand was docked 50 times with full flexibility to the active site grid using AutoDock and Glide. On AutoDock Lamarckian genetic algorithm was selected with medium exhaustiveness, on Glide standard precision was selected. The poses were ranked according to the consensus scores calculated as the average of Autodock score and Glide score of the best poses for each ligand which were selected upon visual evaluation of the results.

For the MD simulations study, the ligand-free (apo) and **5i**-bound CACYP51 models were created and solvated in a water box with a 5-Å layer of water on each face using VMD (v1.9.2) [39], which finally consisted of around 60000 atoms. CHARMM36 force-field was used for the protein and solvent with CMAP corrections, CHARMM General Force-Field (v3.1) via cgenff.paramchem.org server (v1.0) was used for the ligands, and water molecules were modelled using TIP3P water model [40-45]. Particle mesh Ewald (PME) summation was used with grid sizes 114, 103, and 84 and full updates at every 2 fs [46]. Harmonic potential constraints (5 kcal/mol*Å^2) were applied on the backbone atoms of the membrane-embedded residues, Fe^{2+} of heme, and S^- of heme-coordinating cysteine and heme was patched to keep planar. Following an initial 100-step force field minimization, the systems were run for 20 ns at constant temperature (310 K) and pressure (1 atm) (NPT ensemble) with integration time step set to 2 fs, non-bonded cut-off starting at 10 Å, and pair list set to 14 Å using NAMD (v2.10) [47]. SHAKE algorithm [48] was used for hydrogens, and the coordinates were saved every 500 steps.

4.2. Chemistry

The chemicals used in this study were obtained from commercial suppliers. Thin layer chromatography (TLC) was performed using Merck Kieselgel 60 F254 as stationary phase and chloroform-methanol (90:10) as mobile phase to monitor the reactions; the TLC plate spots were inspected under 254 nm UV light. Melting points (mp) were recorded on a Thomas-Hoover capillary melting point apparatus (USA) and uncorrected. ^{1}H NMR (400 MHz) and ^{13}C NMR (100 MHz) spectra were obtained using Varian Mercury 400 FT (USA) NMR spectrometer. LC-MS spectra were recorded with Micromass ZQ mass spectrometer (USA)

connected to Waters Alliance HPLC (USA) with electrospray ionization (ESI+) method and MassLynx 4.1 software. Elemental analyses were performed by LECO 932 CHNS elemental analysis apparatus (USA) and the results are reported as percentages (%). The chemical shifts of the compounds in the NMR spectra are reported as δ (ppm) values using tetramethylsilane as internal reference. The splitting patterns are described as s (singlet), d (doublet), t (triplet), q (quartet), m (multiplet), and dd (doublet of doublet).

4.2.1. Synthesis of the compounds

The title compounds were synthesized as outlined in Scheme 1. Imidazole was *N*-alkylated with commercially obtained 2,2',4-trichloroacetophenone (**1**) to yield 1-(2,4-dichlorophenyl)-2-(1*H*-imidazol-1-yl)ethanone (**2**), which was reduced to 1-(2,4-dichlorophenyl)-2-(1*H*-imidazol-1-yl)ethanol (**3**) with sodium borohydride (NaBH$_4$) and converted to 1-(2,4-dichlorophenyl)-2-(1*H*-imidazol-1-yl)ethanone oxime (**4**) with hydroxylamine hydrochloride (NH$_2$OH.HCl) applying literature methods (see Supporting Information for details) [49, 50].

5a-t and **6a-r** were afforded by Steglich esterification of **3** and **4** with various carboxylic acids [51]. A mixture of *N,N*'-dicyclohexylcarbodiimide (DCC) (1 mmol) and 4-dimethylaminopyridine (DMAP) (0.07 mmol) in dichloromethane (DCM) was added dropwise to a mixture of **3** or **4** (1 mmol) and the proper carboxylic acid (1 mmol) in DCM at 0-5 °C. The mixture was stirred for 0.5 h at 0-5 °C then for an additional 3-6 h at room temperature. The resulting precipitate was filtered off and the filtrate was evaporated to dryness. The residue of **5a-t** was purified via column chromatography (chloroform-methanol 90:10) and that of **6a-r** via crystallization from diethyl ether-methanol. The compounds except **5a**, **6c**, **6e**, **6i**, **6l-n**, **6p**, and **6p** were converted to their HCl salts using ethereal solution of gaseous HCl (gHCl). The structure and purity of the compounds were confirmed via NMR, LC-MS, and elemental analyses.

1-(2,4-dichlorophenyl)-2-(1*H*-imidazol-1-yl)ethyl 4-terphenyl-4-carboxylate (5a): White powder (0.26 g, 47.8% yield); m.p.: 224-25.5 °C; ^{1}H NMR (400 MHz, DMSO-d$_6$): δ=4.62-4.73 (m, 2H, CH$_2$), 6.44 (dd, J_1 = 6.8 Hz, J_2 = 4 Hz, 1H, CH), 7.07 (s, 1H, imidazole H^4), 7.31 (s, 1H, imidazole H^5), 7,37-7.93 (m, 14H, 2,4-dichlorophenyl H^{5,6}, 4-terphenyl H$^{3,5,2',3',5',6',2'',3'',5'',6''}$), 8.01 (m, 1H, 4-terphenyl H$^{4''}$), 8.14 (s, 1H, 2,4-dichlorophenyl H^3), 8.16 (s, 1H, imidazole H^2). ^{13}C NMR (100 MHz, DMSO-d$_6$): δ=49.12 (CH$_2$), 71.39 (OCH), 120.64, 126.52 (2C), 126.85 (2C), 127.22 (2C), 127.35, 127.46 (2C), 127.61, 127.88, 128.88 (2C), 129.01, 130.08 (2C), 132.44,

133.45 (2C), 133.97, 137.43 (2C), 137.53, 139.24, 140.14, 144.71, 164.05 (CO); MS (ESI+) m/z: 535 $[M+Na]^+$ (100%), 513 $[M+H]^+$; Anal. calcd. for $C_{30}H_{22}Cl_2N_2O_2 \cdot H_2O$: C 67.80, H 4.55, N 5.27, found: C 67.59, H 4.12, N 5.44.

1-(2,4-dichlorophenyl)-2-(1*H*-imidazol-1-yl)ethyl 4-phenylbenzoate hydrochloride (5b): Off-white powder (0.25 g, 52.0% yield); m.p.: 218-21 °C; ^{1}H NMR (400 MHz, DMSO-d_6): δ=4.83-4.94 (m, 2H, CH$_2$), 6.53 (dd, J_{AX} = 8.4 Hz, J_{AB} = 4 Hz, 1H, OCH), 7.43-7.54 (m, 5H, 2,4-dichlorophenyl H^{5,6}, 4-phenylbenzoyl H$^{3'-5'}$), 7.66 (s, 1H, imidazole H^4), 7.74-7.77 (m, 3H, 2,4-dichlorophenyl H^3, 4-phenylbenzoyl H$^{2',6'}$), 7.80 (s, 1H, imidazole H^5), 7.84-8.16 (m, 4H, 4-phenylbenzoyl H^{2,3,5,6}), 9.21 (s, 1H, imidazole H^2); ^{13}C NMR (100 MHz, DMSO-d_6): δ=50.51 (CH$_2$), 70.69 (OCH), 119.88, 122.88, 126.99 (2C), 127.04 (2C), 127.10, 128.10, 128.50, 129.06 (3C), 129.24, 130.21 (2C), 132.65, 132.85, 134.32, 136.20, 138.62, 145.42, 164.02 (CO); MS (ESI+) m/z: 440 $[M+4]^+$, 439 $[M+2+H]^+$, 437 $[M+H]^+$, 150 (100%); Anal. calcd. for $C_{24}H_{19}Cl_3N_2O_2$: C 60.84, H 4.04, N 5.91, found: C 60.73, H 4.17, N 6.21.

1-(2,4-dichlorophenyl)-2-(1*H*-imidazol-1-yl)ethyl 2-naphthoate hydrochloride (5c): White powder (0.34 g, 75.4% yield); m.p.: 226-8 °C; ^{1}H NMR (400 MHz, DMSO-d_6): δ=4.90-5.03 (m, 2H, CH$_2$), 6.59 (dd, J_{AX} = 7.6 Hz, J_{AB} = 4 Hz, 1H, OCH), 7.50-7.58 (m, 2H, 2,4-dichlorophenyl H^{5,6}), 7.66-7.75 (m, 3H, 2-naphthoyl H^{4,6,7}), 7.78 (d, J = 2 Hz, 2,4-dichlorophenyl H^3), 7.90 (s, 1H, imidazole H^4), 8.05-8.23 (m, 4H, 2-naphthoyl H^{1,3,5,8}), 8.83 (s, 1H, imidazole H^5), 9.41 (s, 1H, imidazole H^2); ^{13}C NMR (100 MHz, DMSO-d_6): δ=50.67 (CH$_2$), 70.84 (OCH), 119.87, 123.02, 124.75, 125.62, 127.12, 127.74, 128.16, 128.57, 129.01, 129.19, 129.29, 129.49, 131.38, 132.02, 132.73, 132.92, 134.38, 135.33, 136.34, 164.39 (CO); MS (ESI+) m/z: 414 $[M+4]^+$, 413 $[M+2+H]^+$, 411 $[M+H]^+$, 155 (100%); Anal. calcd. for $C_{22}H_{17}Cl_3N_2O_2$: C 59.02, H 3.83, N 6.26, found: C 58.77, H 3.85, N 6.34.

1-(2,4-dichlorophenyl)-2-(1*H*-imidazol-1-yl)ethyl 4-methylthiobenzoate hydrochloride (5d): Pale yellow powder (0.17 g, 37.9% yield); m.p.: 231-3 °C; ^{1}H NMR (400 MHz, DMSO-d_6): δ=2.52 (s, 3H, CH$_3$), 4.79-4.92 (m, 2H, CH$_2$), 6.45-6.48 (q, 1H, CHO), 7.37 (d, J = 8.4 Hz, 2H, 4-methylthiobenzoyl H^{3,5}), 7.42-7.48 (m, 2H, 2,4-dichlorophenyl H^{5,6}), 7.66 (s, 1H, imidazole H^4), 7.72 (d, J = 2 Hz, 1H, 2,4-dichlorophenyl H^3), 7.79 (s, 1H, imidazole H^5), 7.95 (d, J = 8.4 Hz, 2H, 4-methylthiobenzoyl H^{2,6}), 9.27 (s, 1H, imidazole H^2); ^{13}C NMR (100 MHz, DMSO-d_6): δ=13.91 (CH$_3$), 50.57 (CH$_2$), 70.55 (CHO), 119.84, 122.93, 124.12, 125.01 (2C), 128.12, 129.10, 129.27, 129.92 (2C), 132.68, 132.95, 134.34, 136.20, 146.68, 163.97 (CO); MS (ESI+)

m/z: 411 [M+4+H]$^+$, 410 [M+4]$^+$, 408 [M+2]$^+$ (100%); Anal. calcd. for $C_{19}H_{17}Cl_3N_2O_2S.H_2O$: C 48.06, H 3.82, N 8.85, found: C 48.08, H 3.85, N 8.86.

1-(2,4-dichlorophenyl)-2-(1*H*-imidazol-1-yl)ethyl 4-isopropylbenzoate hydrochloride (5e): White powder (0.20 g, 45.6% yield); m.p.: 199-200 °C; ^{1}H NMR (400 MHz, DMSO-d$_6$): δ=1.20 (d, *J* = 7.2 Hz, 6H, CH$_3$), 2.93-2.99 (m, 1H, C**H**(CH$_3$)$_2$), 4.78-4.86 (m, 2H, CH$_2$), 6.45-6.48 (q, 1H, CHO), 7.40-7.48 (m, 4H, 2,4-dichlorophenyl H^{5,6}, 4-isopropylbenzoyl H^{3,5}), 7.65 (s, 1H, imidazole H^4), 7.74 (d, *J* = 2 Hz, 1H, 2,4-dichlorophenyl H^3), 7.78 (s, 1H, imidazole H^5), 7.97 (d, *J* = 8 Hz, 2H, 4-isopropylbenzoyl H^{2,6}), 9.21 (s, 1H, imidazole H^2); ^{13}C NMR (100 MHz, DMSO-d$_6$): δ=23.41 (2C, CH$_3$), 33.52 (**C**H(CH$_3$)$_2$), 50.55 (CH$_2$), 70.51 (CHO), 119.91, 122.91, 126.02, 126.88 (2C), 128.11, 129.03, 129.26, 129.77 (2C), 132.65, 132.97, 134.31, 136.22, 155.07, 164.13 (CO); MS (ESI+) m/z: 407 [M+4+H]$^+$, 406 [M+4]$^+$, 404 [M+2]$^+$ (100%); Anal. calcd. for $C_{21}H_{21}Cl_3N_2O_2$: C 57.35, H 4.81, N 6.37, found: C 57.27, H 5.06, N 6.45.

1-(2,4-dichlorophenyl)-2-(1*H*-imidazol-1-yl)ethyl 4-morpholinobenzoate hydrochloride (5f): Pale yellow powder (0.12 g, 25.7% yield); m.p.: 260-2 °C; ^{1}H NMR (400 MHz, DMSO-d$_6$): δ=3.28 (t, J_{AX} = 4.8 Hz, J_{AY} = 4.8 Hz, 4H, morpholine H$^{3,3',5,5'}$), 3.71 (t, J_{XA} = 4.8 Hz, J_{XB} = 4.8 Hz, 4H, morpholine H$^{2,2',6,6'}$), 4.76-4.88 (m, 2H, CH$_2$), 6.42 (dd, J_1 = 7.2 Hz, J_2 = 4.0 Hz, 1H, CH), 6.98 (d, *J* = 9.2 Hz, 2H, 4-morpholinobenzoyl H^{3,5}), 7.39-7.48 (m, 2H, 2,4-dichlorophenyl H^{5,6}), 7.66 (s, 1H, imidazole H^4), 7.71 (d, *J* = 2.4 Hz, 1H, 2,4-dichlorophenyl H^3), 7.77 (s, 1H, imidazole H^5), 7.87 (d, *J* = 9.2 Hz, 2H, 4-morpholinobenzoyl H^{2,6}), 9.24 (s, 1H, imidazole H^2); ^{13}C NMR (100 MHz, DMSO-d$_6$): δ=46.66 (morpholine C^{3,5}), 50.68 (CH**C**H$_2$), 65.77 (morpholine C^{2,6}), 69.89 (OCH), 113.16 (2C), 116.87, 119.78, 122.91, 128.08, 128.98, 129.24, 131.20 (2C), 132.60, 133.30, 134.21, 136.15, 154.55, 164.00 (CO); MS (ESI+) m/z: 504 [M+Na]$^+$ (100%), 482 [M+H]$^+$; Anal. calcd. for $C_{22}H_{22}Cl_3N_3O_3$: C 54.73, H 4.59, N 8.70, found: C 54.45, H 4.49, N 8.78.

1-(2,4-dichlorophenyl)-2-(1*H*-imidazol-1-yl)ethyl 4-*tert*-butylbenzoate hydrochloride (5g): White powder (0.09 g, 20.0% yield); m.p.: 187-90 °C; ^{1}H NMR (400 MHz, DMSO-d$_6$): δ=1.31 (s, 9H, CH$_3$), 4.81-4.92 (m, 2H, CH$_2$), 6.53 (dd, J_{AX} = 7 Hz, J_{AB} = 4 Hz, 1H, OCH), 7.41-7.50 (m, 2H, 2,4-dichlorophenyl H^{5,6}), 7.58 (d, *J* = 8.8 Hz, 2H, 4-*tert*-butylbenzoyl H^{3,5}), 7.68 (s, 1H, imidazole H^4), 7.77 (d, *J* = 2 Hz, 1H, 2,4-dichlorophenyl H^3), 7.80 (s, 1H, imidazole H^5), 8.00 (d, *J* = 8.8 Hz, 2H, 4-*tert*-butylbenzoyl H^{2,6}), 9.23 (s, 1H, imidazole H^2); ^{13}C NMR (100 MHz, DMSO-d$_6$): δ=31.20 (3C, CH$_3$), 35.39 (**C**(CH$_3$)$_3$), 51.04 (CH$_2$), 70.99 (OCH), 120.39, 123.40,

126.14, 126.22 (2C), 128.59, 129.49, 129.75, 129.99 (2C), 133.13, 133.45, 134.80, 136.70, 157.70, 164.58 (CO); MS (ESI+) m/z: 420 [M+4]$^+$, 419 [M+2+H]$^+$, 417 [M+H]$^+$ (100%); Anal. calcd. for $C_{22}H_{23}Cl_3N_2O_2.1/2H_2O$: C 57.10, H 5.23, N 6.05, found: C 57.39, H 5.32; N, 6.52.

1-(2,4-dichlorophenyl)-2-(1*H*-imidazol-1-yl)ethyl 4-cyanobenzoate hydrochloride (5h): White powder (0.16 g, 39.0% yield); m.p.: 188-90 °C; ^{1}H NMR (400 MHz, DMSO-d$_6$): δ=4.84-4.98 (m, 2H, CH$_2$), 6.51-6.54 (q, 1H, CHO), 7.50-7.82 (m, 5H, 2,4-dichlorophenyl, imidazole H^{4,5}), 8.07 (d, *J* = 8.4 Hz, 2H, 4-cyanobenzoyl H^{3,5}), 8.24 (d, *J* = 8.4 Hz, 2H, 4-cyanobenzoyl H^{2,6}), 9.29 (s, 1H, imidazole H^2); ^{13}C NMR (100 MHz, DMSO-d$_6$): δ=50.49 (CH<u>C</u>H$_2$), 71.48 (CHO), 116.11 (C≡N), 117.94, 119.94, 122.94, 128.15, 129.23, 129.31, 130.27 (2C), 132.33, 132.49, 132.72, 132.91 (2C), 134.50, 136.30, 163.16 (CO); MS (ESI+) m/z: 390 [M+4+H]$^+$, 389 [M+4]$^+$, 387 [M+2]$^+$ (100%); Anal. calcd. for $C_{19}H_{14}Cl_3N_3O_2.H_2O$: C 51.78, H 3.66, N 9.53, found: C 51.37, H 3.56, N 9.58.

1-(2,4-dichlorophenyl)-2-(1*H*-imidazol-1-yl)ethyl 1*H*-indole-2-carboxylate hydrochloride (5i): Pale yellow powder (0.19 g, 41.5% yield); m.p.: 209-11 °C; ^{1}H NMR (400 MHz, DMSO-d$_6$): δ=4.82-4.90 (m, 2H, CHC<u>H</u>$_2$), 6.47-6.50 (m, 1H, OCH), 7.08-7.32 (m, 2H, indole H^{5,6}), 7.36-7.54 (m, 4H, indole H^{3,7}, 2,4-dichlorophenyl H^{5,6}), 7.67-7.69 (m, 2H, imidazole H^4, indole H^4), 7.75 (d, *J* = 2 Hz, 1H, 2,4-dichlorophenyl H^3), 7.87 (s, 1H, imidazole H^5), 9.41 (s, 1H, imidazole H^2), 12.25 (d, *J* = 1.6 Hz, 1H, indole NH); ^{13}C NMR (100 MHz, DMSO-d$_6$): δ=50.70 (CH$_2$), 70.39 (OCH), 109.34, 112.75, 119.87, 120.46, 122.18, 123.02, 125.23, 125.73, 126.60, 128.15, 129.10, 129.26, 132.58, 132.92, 134.37, 136.44, 137.76, 159.46 (CO); MS (ESI+) m/z: 403 [M+4]$^+$, 402 [M+2+H]$^+$, 400 [M+H]$^+$ (100%); Anal. calcd. for $C_{20}H_{16}Cl_3N_3O_2.2/3H_2O$: C 53.53, H 3.89, N 9.36, found: C 53.37, H 3.87, N 9.44.

1-(2,4-dichlorophenyl)-2-(1*H*-imidazol-1-yl)ethyl 3-phenylprop-2-enoate hydrochloride (5j): Off-white powder (0.21 g, 50.0% yield); m.p.: 183-5 °C; ^{1}H NMR (400 MHz, DMSO-d$_6$): δ=4.76-4.78 (m, 2H, CH$_2$), 6.35-6.37 (m, 1H, OCH), 6.73 (d, *J* = 16 Hz, 1H, COCH), 7.30-7.48 (m, 5H, 2,4-dichlorophenyl H^{5,6}, cinnamoyl H$^{3'-5'}$), 7.67 (s, 1H, imidazole H^4), 7.73-7.75 (m, 3H, cinnamoyl H$^{2',6'}$, 2,4-dichlorophenyl H^3), 7.77 (s, 1H, imidazole H^5), 9.19 (s, 1H, imidazole H^2); ^{13}C NMR (100 MHz, DMSO-d$_6$): δ=50.69 (CH$_2$), 69.90 (OCH), 116.84 (COCH), 119.83, 123.07, 128.05, 128.60, 128.92, 128.97, 129.26, 130.92, 132.63, 132.93, 133.78, 134.26 (16C, benzene, imidazole C^{4,5}), 136.31 (<u>C</u>HC$_6$H$_5$), 146.21 (imidazole C^2), 164.60 (CO); MS (ESI+) m/z:

409 [M+Na]$^+$ (100%), 389 [M+2+H]$^+$, 387 [M+H]$^+$; Anal. calcd. for C$_{20}$H$_{17}$Cl$_3$N$_2$O$_2$.2/3H$_2$O: C 55.13, H 4.24, N 6.43, found: C 54.75, H 4.39, N 6.89.

1-(2,4-dichlorophenyl)-2-(1H-imidazol-1-yl)ethyl 4-ethylbenzoate hydrochloride (5k): Off-white powder (0.23 g, 53.5% yield); m.p.: 198-9 °C; ^{1}H NMR (400 MHz, DMSO-d$_6$): δ=1.19 (t, J_1 = 7.6 Hz, J_2 = 7.2 Hz, 3H, CH$_3$), 2.66-2.71 (q, 2H, CH$_2$CH$_3$), 4.82-4.96 (m, 2H, CHCH$_2$), 6.50 (dd, J_1 = 7.6 Hz, J_2 = 4.0 Hz, 1H, CH), 7.38 (d, J = 8.4 Hz, 2H, 4-ethylbenzoyl H^{3,5}), 7.47-7.67 (m, 3H, 2,4-dichlorophenyl H^{5,6}, imidazole H^4), 7.71-7.81 (m, 2H, 2,4-dichlorophenyl H^3, imidazole H^5), 7.98 (d, J = 8.4 Hz, 2H, 4-ethylbenzoyl H^{2,6}), 9.31 (s, 1H, imidazole H^2); ^{13}C NMR (100 MHz, DMSO-d$_6$): δ=15.15 (CH$_3$), 28.20 (CH$_2$CH$_3$), 51.56 (CHCH$_2$), 70.52 (OCH), 119.80, 122.93, 125.87, 128.12, 128.31 (2C), 129.09, 129.25, 129.74 (2C), 132.68, 132.98, 134.32, 136.19, 150.61, 164.19 (CO); MS (ESI+) m/z: 411 [M+Na]$^+$ (100%), 389 [M+H]$^+$; Anal. calcd. for C$_{20}$H$_{19}$Cl$_3$N$_2$O$_2$: C 56.43, H 4.50, N 6.58, found: C 56.72, H 4.38, N 6.97.

1-(2,4-dichlorophenyl)-2-(1H-imidazol-1-yl)ethyl cyclohexanecarboxylate hydrochloride (5l): Off-white powder (0.20 g, 48.4% yield); m.p.: 149-150.5 °C; ^{1}H NMR (400 MHz, DMSO-d$_6$): δ=1.14-2.39 (m, 11H, cyclohexane), 4.68 (d, J = 6.0 Hz, CHCH$_2$N), 6.23 (t, J_1 = 5.6 Hz, J_2 = 5.6 Hz, 1H, CHO), 7.28 (d, J = 8.8 Hz, 1H, 2,4-dichlorophenyl H^6), 7.48 (dd, J_1 = 8.8 Hz, J_2 = 2 Hz, 1H, 2,4-dichlorophenyl H^5), 7.66-7.72 (m, 3H, imidazole H^{4,5}, 2,4-dichlorophenyl H^3), 9.12 (s, 1H, imidazole H^2); ^{13}C NMR (100 MHz, DMSO-d$_6$): δ=24.57 (cyclohexane C^3), 24.64 (cyclohexane C^5), 25.11 (cyclohexane C^4), 28.09 (cyclohexane C^2), 28.23 (cyclohexane C^6), 41.69 (cyclohexane C^1), 50.51 (CHCH$_2$N), 69.41 (CHO), 119.80, 122.87, 128.03, 128.89, 129.20, 132.67, 132.97, 134.21, 136.14, 173.39 (CO); MS (ESI+) m/z: 372 [M+4+H]$^+$, 370 [M+2+H]$^+$, 368 [M+H]$^+$ (100%); Anal. calcd. for C$_{18}$H$_{21}$Cl$_3$N$_2$O$_2$: C 53.55, H 5.24, N 6.94, found: C 53.14, H 5.49, N 7.06.

1-(2,4-dichlorophenyl)-2-(1H-imidazol-1-yl)ethyl 4-(*tert*-butoxycarbonylamino)butanoate hydrochloride (5m): White powder (0.17 g, 35.5% yield); m.p.: 136-8 °C; ^{1}H NMR (400 MHz, DMSO-d$_6$): δ=1.35 (s, 9H, CH$_3$), 1.55-1.60 (m, 2H, COCH$_2$CH$_2$), 2.38 (t, J_1 = 7.6 Hz, J_2 = 7.2 Hz, COCH$_2$), 2.84-2.89 (q, 2H, CH$_2$NH), 4.67-4.69 (m, 2H, CHCH$_2$), 6.25 (t, J_1 = 5.6 Hz, J_2 = 5.2 Hz, 1H, OCH), 6.83 (t, J_1 = 5.6 Hz, J_2 = 5.6 Hz, 1H, NH), 7.26 (d, J = 8.4 Hz, 1H, 2,4-dichlorophenyl H^6), 7.44 (dd, J_1 = 8.4 Hz, J_2 = 2 Hz, 1H, 2,4-dichlorophenyl H^5), 7.63-7.71 (m, 3H, imidazole H^{4,5}, 2,4-dichlorophenyl H^3), 9.06 (s, 1H, imidazole H^2); ^{13}C NMR (100 MHz, DMSO-d$_6$): δ=24.50 (COCH$_2$CH$_2$), 28.14 (3C, CH$_3$), 30.50 (COCH$_2$), 39.90 (CH$_2$NH), 50.50 (CHCH$_2$), 69.50

(OCH), 77.42 ($\underline{C}(CH_3)_3$), 119.81, 122.85, 127.87, 128.89, 129.12, 132.51, 132.74, 134.12, 136.10, 155.53 (NHCO), 171.23 (2C, $\underline{C}OCH_2$, NHCO); MS (ESI+) m/z: 464 $[M+Na]^+$ (100%), 444 $[M+2+H]^+$, 442 $[M+H]^+$; Anal. calcd. for $C_{20}H_{26}Cl_3N_3O_4$: C 50.17, H 5.47, N 8.78, found: C 49.78, H 5.69, N 8.92.

1-(2,4-dichlorophenyl)-2-(1*H*-imidazol-1-yl)ethyl 2,4-dichlorobenzoate hydrochloride (5n):
Pale yellow powder (0.30 g, 63.5%); m.p.: 140-2 °C; ^{1}H NMR (400 MHz, DMSO-d_6): δ=4.82-4.94 (m, 2H, CH_2), 6.52 (dd, J_1 = 7.2 Hz, J_2 = 4 Hz, 1H, OCH), 7.47-7.53 (m, 2H, 2,4-dichlorophenyl H^{5,6}), 7.62 (dd, J_1 = 8.4 Hz, J_2 = 2 Hz, 1H, 2,4-dichlorobenzoyl H^5), 7.65 (s, 1H, imidazole H^4), 7.74 (s, 1H, imidazole H^5), 7.76 (d, J = 2 Hz, 1H, 2,4-dichlorobenzoyl H^3), 7.80 (d, J = 2 Hz, 1H, 2,4-dichlorophenyl H^3), 8.06 (d, J = 8.4 Hz, 1H, 2,4-dichlorobenzoyl H^6), 9.20 (s, 1H, imidazole H^2); ^{13}C NMR (100 MHz, DMSO-d_6): δ=50.39 (CH_2), 71.49 (CH), 120.10, 122.84, 126.80, 127.82, 128.15, 129.30 (2C), 130.71, 132.41, 132.87, 133.28, 133.94, 134.51, 136.28, 138.16, 162.31 (CO); MS (ESI+) m/z: 457 $[M+6+Na]^+$, 455 $[M+4+Na]^+$, 453 $[M+2+Na]^+$ (100%), 451 $[M+Na]^+$; Anal. calcd. for $C_{18}H_{13}Cl_5N_2O_2 1/2H_2O$: C 45.46, H 2.97, N 5.89, found: C 45.19, H 2.76, N 6.24.

1-(2,4-dichlorophenyl)-2-(1*H*-imidazol-1-yl)ethyl 4-methoxybenzoate hydrochloride (5o):
Pale yellow powder (0.22 g, 51.2% yield); m.p.: 176 °C; ^{1}H NMR (400 MHz, DMSO-d_6): δ=2.48 (s, 3H, CH_3), 4.77-4.88 (m, 2H CHCH_2), 6.43-6.46 (q, 1H, CHO), 7.06 (d, J = 8.8 Hz, 2H, 4-methoxybenzoyl H^{3,5}), 7.39-7.49 (m, 2H, 2,4-dichloropheyl H^{5,6}), 7.64 (s, 1H, imidazole H^4), 7.73 (d, J = 2 Hz, 1H, 2,4-dichlorophenyl H^3), 7.76 (s, 1H, imidazole H^5), 8.00 (d, J = 9.2 Hz, 2H, 4-methoxybenzoyl H^{2,6}), 9.18 (s, 1H, imidazole H^2); ^{13}C NMR (100 MHz, DMSO-d_6): δ=50.60 (CHCH_2), 55.64 (CH_3), 70.34 (CHO), 114.22 (2C), 119.90, 120.46, 122.90, 128.11, 129.04, 129.25, 131.79 (2C), 132.64, 133.08, 134.29, 136.21, 163.74, 163.85 (CO); MS (ESI+) m/z: 395 $[M+4+H]^+$, 394 $[M+4]^+$, 392 $[M+2]^+$ (100%); Anal. calcd. for $C_{19}H_{17}Cl_3N_2O_3.H_2O$: C 51.20, H 4.30, N 6.28, found: C 51.37, H 4.39, N 6.40.

1-(2,4-dichlorophenyl)-2-(1*H*-imidazol-1-yl)ethyl 4-phenylbutanoate hydrochloride (5p):
Off-white powder (0.11 g, 26.0% yield); m.p.: 148-50 °C; ^{1}H NMR (400 MHz, DMSO-d_6): δ=1.72-1.80 (m, 2H, $C\underline{H}_2CH_2C_6H_5$), 2.38 (t, J_1 = 7.6 Hz, J_2 = 7.2 Hz, 2H, COCH_2), 2.50-2.52 (m, 2H, $C\underline{H}_2C_6H_5$, overlaps with DMSO), 4.68 (d, J = 6 Hz, 2H, CH$C\underline{H}_2$), 6.26 (t, J_1 = 5.6 Hz, J_2 = 5.6 Hz, 1H, OCH), 7.11-7.29 (m, 6H, 4-phenylbutanoyl H$^{3'-5'}$, imidazole H^{4,5}, 2,4-dichlorobenzoyl H^6), 7.46-7.72 (m, 4H, 2,4-dichlorobenzoyl H^{3,5}, 4-phenylbutanoyl H$^{2',6'}$), 9.11 (s, 1H,

imidazole H^2); ^{13}C NMR (100 MHz, DMSO-d$_6$): δ=25.79 (C̲H$_2$CH$_2$C$_6$H$_5$), 32.57 (COC̲H$_2$), 34.09 (C̲H$_2$C$_6$H$_5$), 50.23 (CHC̲H$_2$), 69.55 (OCH), 119.77, 122.86, 125.85, 127.95, 128.21 (2C), 128.28 (2C), 128.99, 129.18, 132.63, 132.81, 134.23, 136.12, 141.07, 171.31 (CO); MS (ESI+) m/z: 425 [M+Na]$^+$ (100%), 406 [M+4]$^+$, 405 [M+2+H]$^+$, 403 [M+H]$^+$; Anal. calcd. for C$_{21}$H$_{21}$Cl$_3$N$_2$O$_2$: C 57.36, H 4.81, N 6.37, found: C 57.07, H 5.03, N 6.59.

1-(2,4-dichlorophenyl)-2-(1*H*-imidazol-1-yl)ethyl cyclopentanecarboxylate hydrochloride (5q): Off-white powder (0.20 g, 51.0% yield); m.p.: 188-90 °C; ^{1}H NMR (400 MHz, DMSO-d$_6$): δ=1.53-1.84 (m, 9H, cyclopentane), 4.72 (d, J = 5.6 Hz, 2H, CHC̲H$_2$N), 6.25 (t, J_1 = 5.6 Hz, J_2 = 6.4 Hz, 1H, CHO), 7.30 (d, J = 8.4 Hz, 1H, 2,4-dichlorophenyl H^6), 7.50 (dd, J_1 = 8.4 Hz, J_2 = 2 Hz, 1H, 2,4-dichlorophenyl H^5), 7.68-7.72 (m, 3H, imidazole H^{4,5}, 2,4-dichlorophenyl H^3), 9.20 (s, 1H, imidazole H^2); ^{13}C NMR (100 MHz, DMSO-d$_6$): δ=25.18 (2C, cyclopentane C^{3,4}), 29.07 (cyclopentane C^2), 29.24 (cyclopentane C^5), 42.70 (cyclopentane C^1), 50.52 (CHC̲H$_2$N), 69.53 (CHO), 119.72, 122.89, 128.04, 128.86, 129.22, 132.68, 132.97, 134.22, 136.13, 174.10 (CO); MS (ESI+) m/z: 357 [M+4+H]$^+$, 356 [M+4]$^+$, 354 [M+2]$^+$ (100%); Anal. calcd. for C$_{17}$H$_{19}$Cl$_3$N$_2$O$_2$: C 52.39, H 4.91, N 7.19, found: C 52.52, H 5.19, N 7.41.

1-(2,4-dichlorophenyl)-2-(1*H*-imidazol-1-yl)ethyl 4-nitrobenzoate hydrochloride (5r): Yellow powder (0.22 g, 50.5% yield); m.p.: 218 °C; ^{1}H NMR (400 MHz, DMSO-d$_6$): δ=4.83-4.97 (m, 2H, CH$_2$), 6.50-6.53 (q, 1H, CHO), 7.48-7.75 (m, 4H, 2,4-dichlorophenyl, imidazole H^4), 7.80 (s, 1H, imidazole H^5), 8.29-8.35 (m, 4H, 4-nitrobenzoyl), 9.28 (s, 1H, imidazole H^2); ^{13}C NMR (100 MHz, DMSO-d$_6$): δ=50.48 (CH$_2$), 71.60 (CHO), 119.92, 122.96, 123.90 (2C), 128.15, 129.24, 129.32, 131.15 (2C), 132.44, 132.75, 133.79, 134.52, 136.30, 150.63, 162.90 (CO); MS (ESI+) m/z: 409 [M+4]$^+$, 408 [M+2+H]$^+$, 406 [M+H]$^+$ (100%); Anal. calcd. for C$_{21}$H$_{21}$Cl$_3$N$_2$O$_2$.1/2H$_2$O: C 47.86, H 3.35, N 9.30, found: C 47.87, H 3.28, N 9.44.

1-(2,4-dichlorophenyl)-2-(1*H*-imidazol-1-yl)ethyl 3-benzoylpropanoate hydrochloride (5s): Off-white powder (0.30 g, 66.0% yield); m.p.: 159-61 °C; ^{1}H NMR (400 MHz, DMSO-d$_6$): δ=2.75-2.78 (m, 2H, COCH$_2$), 3.31-3.35 (q, 2H, C̲H$_2$COC$_6$H$_5$), 4.70 (d, J = 5.6 Hz, CHC̲H$_2$), 6.27 (t, J_1 = 5.6 Hz, J_2 = 5.2 Hz, 1H, OCH), 7.32 (d, J = 8.4 Hz, 1H, 2,4-dichlorophenyl H^6), 7.46 (dd, J_1 = 8.4 Hz, J_2 = 2 Hz, 1H, 2,4-dichlorophenyl H^5), 7.52-7.69 (m, 5H, 3-benzoylpropanoyl H$^{3'-5'}$, imidazole H^{4,5}), 7.72 (d, J = 2 Hz, 1H, 2,4-dichlorophenyl H^3), 7.95-7.97 (m, 2H, 3-benzoylpropanoyl H$^{2',6'}$), 9.12 (s, 1H, imidazole H^2); ^{13}C NMR (100 MHz, DMSO-d$_6$): δ=27.70 (COC̲H$_2$), 32.87 (C̲H$_2$COC$_6$H$_5$), 50.54 (CHC̲H$_2$), 69.74 (OCH), 119.73, 122.81, 127.80 (3C),

128.65 (2C), 129.05, 129.06, 132.48, 132.65, 133.28, 134.15, 136.04, 136.08, 171.06 (OCO), 198.05 ($\underline{C}$OC$_6$H$_5$); MS (ESI+) m/z: 439 [M+Na]$^+$ (100%), 420 [M+4]$^+$, 419 [M+2+H]$^+$, 417 [M+H]$^+$; Anal. calcd. for C$_{21}$H$_{19}$Cl$_3$N$_2$O$_3$: C 55.59, H 4.22, N 6.17, found: C 55.18, H 4.37, N 6.47.

1-(2,4-dichlorophenyl)-2-(1*H*-imidazol-1-yl)ethyl 4-trifluoromethylbenzoate hydrochloride (5t): Pale yellow powder (0.19 g, 40.8% yield); m.p.: 187-90 °C; ^{1}H NMR (400 MHz, DMSO-d$_6$): δ=4.87-5.01 (m, 2H, CH$_2$), 6.54-6.57 (q, 1H, CHO), 7.49-7.55 (m, 2H, 2,4-dichlorophenyl H^{5,6}), 7.69 (s, 1H, imidazole H^4), 7.77 (d, *J* = 2 Hz, 1H, 2,4-dichlorophenyl H^3), 7.85 (s, 1H, imidazole H^5), 7.95 (d, *J* = 8.4 Hz, 2H, 4-trifluoromethylbenzoyl H^{3,5}), 8.30 (d, *J* = 8.4 Hz, 2H, 4-trifluoromethylbenzoyl H^{2,6}), 9.34 (s, 1H, imidazole H^2); ^{13}C NMR (100 MHz, DMSO-d$_6$): δ=50.49 (CH$_2$), 71.36 (CHO), 119.86, 122.24, 122.97, 124.95, 125.85, 125.89, 128.14, 129.25, 129.30, 130.54, 132.17, 132.55, 132.75, 133.24, 133.56, 134.48, 136.27, 163.26 (CO); MS (ESI+) m/z: 432 [M+4]$^+$, 431 [M+2+H]$^+$, 429 [M+H]$^+$ (100%); Anal. calcd. for C$_{19}$H$_{13}$Cl$_3$F$_3$N$_2$O$_2$: C 49.00, H 3.03, N 6.02, found: C 48.65, H 3.23, N 6.07.

1-(2,4-dichlorophenyl)-2-(1*H*-imidazol-1-yl)ethanone *O*-(4-terphenylcarbonyl) oxime hydrochloride (6a): Pale yellow powder (0.07 g, 13.0% yield); m.p.: 265-8 °C; ^{1}H NMR (400 MHz, DMSO-d$_6$): δ=6.12 (s, 2H, CH$_2$), 7.38-7.52 (m, 4H, 4-terphenyl H$^{3"-5"}$, imidazole H^4), 7.56 (dd, *J$_1$* = 8 Hz, *J$_2$* = 2 Hz, 1H, 2,4-dichlorophenyl H^5), 7.61 (s, 1H, imidazole H^5), 7.68 (d, *J* = 8.4 Hz, 1H, 2,4-dichlorophenyl H^6), 7.74-7.76 (m, 2H, 4-terphenyl H$^{2",6"}$), 7.84 (d, *J* = 8.4 Hz, 2H, 4-terphenyl H$^{3',5'}$), 7.91 (d, *J* = 8.4 Hz, 2H, 4-terphenyl H$^{2',6'}$), 7.99 (d, *J* = 8.8 Hz, 2H, 4-terphenyl H^{3,5}), 8.27 (d, *J* = 8.4 Hz, 2H, 4-terphenyl H^{2,6}), 9.11 (s, 1H, imidazole H^2); MS (ESI+) m/z: 529 [M+4]$^+$, 528 [M+2+H]$^+$, 526 [M+H]$^+$ (100%); Anal. calcd. for C$_{30}$H$_{22}$Cl$_3$N$_3$O$_2$.H$_2$O: C 62.03, H, 4.16, N 7.23, found: C 62.04, H 4.10, N 7.44.

1-(2,4-dichlorophenyl)-2-(1*H*-imidazol-1-yl)ethanone *O*-(2-naphthoate) oxime hydrochloride (6b): White powder (0.16 g, 33.8% yield); m.p.: 157-9 °C; ^{1}H NMR (400 MHz, DMSO-d$_6$): δ=5.80 (s, 2H, CH$_2$), 7.56 (dd, *J$_1$* = 8.4 Hz, *J$_2$* = 1.6 Hz, 1H, 2,4-dichlorophenyl H^5), 7.60-7.70 (m, 10H, naphthoyl, 2,4-dichlorophenyl H^{3,6}, imidazole H^4), 8.27 (s, 1H, imidazole H^2), 9.35 (s, 1H, imidazole H^2); ^{13}C NMR (100 MHz, DMSO-d$_6$): δ=50.40 (CH$_2$), 120.14, 123.10, 123.80, 124.50, 127.37, 128.12, 128.50, 128.88, 129.18 (3C), 129.22 (2C), 130.34, 130.91, 131.88, 135.25, 136.02, 136.61, 159.42 (CNO), 161.88 (CO); MS (ESI+) m/z: 446 [M+Na]$^+$

(100%), 426 [M+2+H]$^+$, 424 [M+H]$^+$; Anal. calcd. for $C_{22}H_{16}Cl_3N_3O_2.1/2H_2O$: C 56.25, H 3.65, N 8.95, found: C 56.66, H 3.39, N 9.29.

1-(2,4-dichlorophenyl)-2-(1*H*-imidazol-1-yl)ethanone *O*-(4-phenylbenzoyl) oxime (6c): Off-white powder (0.23 g, 50.0% yield); m.p.: 129-31 °C; ^{1}H NMR (400 MHz, DMSO-d$_6$): δ=5.82 (s, 2H, CH$_2$), 6.74 (s, 1H, imidazole H^4), 7.07 (s, 1H, imidazole H^5), 7.46-7.49 (m, 2H, 2,4-dichlorophenyl H^5, 4-phenylbenzoyl H$^{4'}$), 7.52-7.56 (m, 3H, 2,4-dichlorophenyl H^6, 4-phenylbenzoyl H$^{3',5'}$), 7.63 (s, 1H, imidazole H^2), 7.68 (d, *J* = 2 Hz, 1H, 2,4-dichlorophenyl H^3), 7.79-7.81 (m, 2H, 4-phenylbenzoyl H$^{2',6'}$), 7.92 (d, *J* = 8.8 Hz, 2H, 4-phenylbenzoyl H^{3,5}), 8.27 (d, *J* = 8.4 Hz, 2H, 4-phenylbenzoyl H^{3,5}); ^{13}C NMR (100 MHz, DMSO-d$_6$): δ=44.94 (CH$_2$), 120.24, 126.46, 127.05 (3C), 127.18 (2C), 127.28, 128.40, 128.59, 128.85, 129.12 (2C), 129.63, 130.36 (2C), 132.12, 132.86, 135.42, 138.20, 145.55, 162.12 (CNO), 163.40 (CO); MS (ESI+) m/z: 453 [M+4]$^+$, 452 [M+2+H]$^+$, 450 [M+H]$^+$, 69 (100%); Anal. calcd. for $C_{24}H_{17}Cl_2N_3O_2$: C 64.01, H 3.81, N 9.33, found: C 63.82, H 3.60, N 9.39.

1-(2,4-dichlorophenyl)-2-(1*H*-imidazol-1-yl)ethanone *O*-(1*H*-indole-2-carbonyl) oxime hydrochloride (6d): White powder (0.19 g, 43.0% yield); m.p.: 149-50.5 °C; ^{1}H NMR (400 MHz, DMSO-d$_6$): δ=6.20 (s, 2H, CH$_2$), 7.15 (t, J_1 = 7.6 Hz, J_2 = 7.6 Hz, 1H, indole H^5), 7.35 (t, J_1 = 7.6 Hz, J_2 = 7.6 Hz, 1H, indole H^6), 7.55-7.59 (m, 4H, 2,4-dichlorophenyl H^5, indole H^{4,7}, imidazole H^4), 7.68-7.76 (m, 4H, 2,4-dichlorophenyl H^{3,5}, indole H^{4,7}, imidazole H^5), 9.28 (s, 1H, imidazole H^2), 12.42 (s, 1H, indole NH); ^{13}C NMR (100 MHz, DMSO-d$_6$): δ=47.40 (CH$_2$), 109.96, 112.83, 120.17, 120.64, 122.28, 123.00, 124.10, 125.50, 126.63, 127.81, 128.81, 129.18, 132.72, 132.85, 136.10, 136.73, 138.12, 157.57 (CNO), 160.27 (CO); MS (ESI+) m/z: 418 [M+4+H]$^+$, 416 [M+2+H]$^+$, 414 [M+H]$^+$ (100%); Anal. calcd. for $C_{20}H_{15}Cl_3N_4O_2$: C 53.41, H 3.36, N 12.46, found: C 52.99, H 3.54, N 12.20.

1-(2,4-dichlorophenyl)-2-(1*H*-imidazol-1-yl)ethanone *O*-(4-*tert*-butylbenzoyl) oxime (6e): White powder (0.10 g, 22.7% yield); m.p.: 103-4 °C; ^{1}H NMR (400 MHz, DMSO-d$_6$): δ=1.32 (s, 9H, CH$_3$) 5.77 (s, 2H, CH$_2$), 6.77 (s, 1H, imidazole H^4), 7.07 (s, 1H, imidazole H^5), 7.45 (dd, J_1 = 8.4 Hz, J_2 = 2 Hz, 1H, 2,4-dichlorophenyl H^5), 7.51 (d, *J* = 8 Hz, 1H, 2,4-dichlorophenyl H^6), 7.62 (d, *J* = 8.8 Hz, 2H, 4-*tert*-butylbenzoyl H^{3,5}), 7.66 (d, *J* = 2 Hz, 1H, 2,4-dichlorophenyl H^3), 7.68 (s, 1H, imidazole H^2), 8.09 (d, *J* = 8 Hz, 2H, 4-*tert*-butylbenzoyl H^{2,6}); ^{13}C NMR (100 MHz, DMSO-d$_6$): δ=30.74 (3C, CH$_3$), 34.97 (<u>C</u>(CH$_3$)$_3$), 45.03 (CH$_2$), 120.38, 124.95, 125.89 (2C), 127.32, 127.96, 128.87, 129.62 (3C), 132.18, 132.86, 135.43, 138.12, 157.37, 162.18 (CNO),

163.11 (CO); MS (ESI+) m/z: 433 [M+4]$^+$, 432 [M+2+H]$^+$, 430 [M+H]$^+$ (100%); Anal. calcd. for C$_{22}$H$_{21}$Cl$_2$N$_3$O$_2$.1/2H$_2$O: C 60.15, H 5.04, N 9.56, found: C 59.90, H 4.98, N 9.68.

1-(2,4-dichlorophenyl)-2-(1*H*-imidazol-1-yl)ethanone   *O*-(2,4-dichlorobenzoyl)   oxime hydrochloride (6f): White powder (0.23 g, 48.5% yield); m.p.: 135-7 °C; ^{1}H NMR (400 MHz, DMSO-d$_6$): δ=6.03 (s, 2H, CH$_2$), 7.52 (s, 1H, imidazole H^4), 7.56 (dd, J_1 = 8 Hz, J_2 = 2 Hz, 1H, 2,4-dichlorophenyl H^5), 7.61 (s, 1H, imidazole H^5), 7.67-7.70 (m, 2H, 2,4-dichlorophenyl H^6, 2,4-dichlorobenzoyl H^5), 7.73 (d, J = 2 Hz, 1H, 2,4-dichlorophenyl H^3), 7.92 (d, J = 2 Hz, 1H, 2,4-dichlorobenzoyl H^3), 8.16 (d, J = 8.4 Hz, 1H, 2,4-dichlorobenzoyl H^6), 9.23 (s, 1H, imidazole H^2); ^{13}C NMR (100 MHz, DMSO-d$_6$): δ=47.48 (CH$_2$), 120.04, 122.94, 126.34, 127.82, 127.92, 128.44, 129.18, 130.79, 132.64, 132.71, 133.29, 133.90, 136.20, 136.76, 138.40, 160.46 (CNO), 161.58 (CO); MS (ESI+) m/z: 468 [M+4+Na]$^+$, 466 [M+2+Na]$^+$, 464 [M+Na]$^+$, 153 (100%); Anal. calcd. for C$_{18}$H$_{12}$Cl$_5$N$_3$O$_2$.H$_2$O: C 43.45, H 2.84, N 8.45, found: C 43.11, H 2.69, N 8.89.

1-(2,4-dichlorophenyl)-2-(1*H*-imidazol-1-yl)ethanone   *O*-(4-methylthiobenzoyl)   oxime hydrochloride (6g): Pale yellow powder (0.20 g, 43.1% yield); m.p.: 122-3 °C; ^{1}H NMR (400 MHz, DMSO-d$_6$): δ=2.56 (CH$_3$), 6.11 (CH$_2$), 7.44 (d, J = 8 Hz, 2H, 4-methylthiobenzoyl H^{3,5}), 7.52-7.55 (m, 2H, 2,4-dichlorophenyl H^{5,6}), 7.63 (s, 1H, imidazole H^4), 7.68-7.71 (m, 2H, 2,4-dichlorophenyl H^3, imidazole H^5), 8.06 (d, J = 8.4 Hz, 2H, 4-methylthiobenzoyl H^{2,6}), 9.25 (s, 1H, imidazole H^2); ^{13}C NMR (100 MHz, DMSO-d$_6$): δ=13.89 (CH$_3$), 47.35 (CH$_2$), 120.01, 122.96, 122.99, 125.12 (2C), 127.76, 128.76, 129.12, 130.04 (2C), 132.70, 132.78, 136.05, 136.67, 147.14, 160.72 (CNO), 161.80 (CO); MS (ESI+) m/z: 423 [M+4]$^+$, 422 [M+2+H]$^+$, 420 [M+H]$^+$ (100%); Anal. calcd. for C$_{19}$H$_{16}$Cl$_3$N$_3$O$_2$S.H$_2$O: C 48.06, H 3.82, N 8.85, found: C 48.08, H 3.85, N 8.86.

1-(2,4-dichlorophenyl)-2-(1*H*-imidazol-1-yl)ethanone   *O*-(4-ethylbenzoyl)   oxime hydrochloride (6h): Pale yellow powder (0.21 g, 48.4% yield); m.p.: 159-61 °C; ^{1}H NMR (400 MHz, DMSO-d$_6$): δ=1.12 (t, J_1 = 7.6 Hz, J_2 = 7.6 Hz, 3H, CH$_3$), 2.58-2.64 (q, 2H, C**H$_2$**CH$_3$), 5.69 (s, 2H, CH$_2$N), 7.31 (d, J = 7.6 Hz, 2H, 4-ethylbenzoyl H^{3,5}), 7.51 (d, J = 8 Hz, 2H, 4-ethylbenzoyl H^{2,6}), 7.66-7.72 (m, 3H, 2,4-dichlorophenyl H^{5,6}, imidazole H^4), 7.76 (s, 1H, imidazole H^5), 7.87 (d, J = 2 Hz, 1H, 2,4-dichlorophenyl H^3), 9.24 (s, 1H, imidazole H^2); ^{13}C NMR (100 MHz, DMSO-d$_6$): 14.94 (CH$_3$), 28.13 (**C**H$_2$CH$_3$), 50.43 (CH$_2$N), 120.07, 123.08, 124.65, 128.06, 128.47, 128.52 (2C), 129.03 (2C), 129.16, 130.25, 131.79, 135.92, 136.56, 150.80, 158.96 (CNO),

161.79 (CO); MS (ESI+) m/z: 407 [M+4+H]$^+$, 405 [M+2+H]$^+$, 403 [M+H]$^+$ (100%); Anal. calcd. for $C_{20}H_{18}Cl_3N_3O_2 \cdot H_2O$: C 52.59, H 4.41, N 9.20, found: C 52.38, H 4.55, N 9.32.

1-(2,4-dichlorophenyl)-2-(1*H*-imidazol-1-yl)ethanone *O*-(4-cyanobenzoyl) oxime (6i): Yellow powder (0.17 g, 42.7% yield); m.p.: 103-5 °C; ^{1}H NMR (400 MHz, DMSO-d$_6$): δ=5.80 (CH$_2$N), 6.72 (s, 1H, imidazole H^4), 7.03 (s, 1H, imidazole H^5), 7.46 (dd, J_1 = 8 Hz, J_2 = 2 Hz, 1H, 2,4-dichlorophenyl H^5), 7.50 (d, J = 8 Hz, 1H, 2,4-dichlorophenyl H^6), 7.57 (s, 1H, imidazole H^2), 7.67 (d, J = 2 Hz, 1H, 2,4-dichlorophenyl H^3), 8.11 (d, J = 8.4 Hz, 2H, 4-cyanobenzoyl H^{3,5}), 8.34 (d, J = 8.4 Hz, 2H, 4-cyanobenzoyl H^{2,6}); ^{13}C NMR (100 MHz, DMSO-d$_6$): δ=44.94 (CH$_2$), 116.23 (C≡N), 117.92, 120.18, 127.31, 128.61, 128.89, 129.37, 130.36 (2C), 131.74, 132.06, 132.79, 132.99 (2C), 135.51, 138.22, 161.19 (CNO), 164.35 (CO); MS (ESI+) m/z: 403 [M+4+H]$^+$, 402 [M+4]$^+$, 400 [M+2]$^+$ (100%); Anal. calcd. for $C_{19}H_{12}Cl_2N_4O_2 \cdot 1/2H_2O$: C 55.90, H 3.21, N 13.72, found: C 55.66, H 3.36, N 13.56.

1-(2,4-dichlorophenyl)-2-(1*H*-imidazol-1-yl)ethanone *O*-(4-chlorobenzoyl) oxime hydrochloride (6j): White powder (0.19 g, 42.9% yield); m.p.: 121-2.5 °C; ^{1}H NMR (400 MHz, DMSO-d$_6$): δ=6.13 (CH$_2$), 7.52-7.55 (m, 2H, 2,4-dichlorophenyl H^{5,6}), 7.63 (s, 1H, imidazole H^4) 7.68-7.71 (m, 4H, 2,4-dichlorophenyl H^3, 4-chlorophenyl H^{3,5}, imidazole H^5), 8.18 (d, J = 8.4 Hz, 2H, 4-dichlorophenyl H^{2,6}), 9.25 (s, 1H, imidazole H^2); ^{13}C NMR (100 MHz, DMSO-d$_6$): δ=47.34 (CH$_2$), 120.08, 122.96, 126.31, 127.79, 128.60, 129.16, 129.28 (2C), 131.61 (2C), 132.67, 132.76, 136.13, 136.70, 139.39, 161.26 (CNO), 161.32 (CO); MS (ESI+) m/z: 413 [M+6]$^+$, 412 [M+4+H]$^+$, 410 [M+2+H]$^+$, 408 [M+H]$^+$ (100%); Anal. calcd. for $C_{18}H_{13}Cl_4N_3O_2 \cdot H_2O$: C 46.68, H 3.26, N 9.07, found: C 46.72, H 3.41, N 9.21.

1-(2,4-dichlorophenyl)-2-(1*H*-imidazol-1-yl)ethanone *O*-(4-nitrobenzoyl) oxime hydrochloride (6k): White powder (0.24 g, 52.7% yield); m.p.: 134-6 °C; ^{1}H NMR (400 MHz, DMSO-d$_6$): δ=6.18 (s, 2H, CH$_2$), 7.53-7.56 (m, 2H, 2,4-dichlorophenyl H^5, imidazole H^4), 7.65 (s, 1H, imidazole H^5), 7.70-7.72 (m, 2H, 2,4-dichlorophenyl H^{3,6}), 8.38-8.44 (m, 4H, 4-nitrobenzoyl), 9.29 (s, 1H, imidazole H^2); ^{13}C NMR (100 MHz, DMSO-d$_6$): δ=47.36 (CH$_2$), 120.09, 122.98, 124.02 (2C), 127.82, 128.45, 129.20, 131.30 (2C), 132.66, 132.74, 133.00, 136.22, 136.72, 150.76, 160.78 (CNO), 161.86 (CO); (ESI+) m/z: 422 [M+4]$^+$, 421 [M+2+H]$^+$, 419 [M+H]$^+$ (100%); Anal. calcd. for $C_{18}H_{13}Cl_3N_4O_4$: C 47.44, H 2.88, N 12.30, found: C 47.08, H 3.03, N 12.26.

1-(2,4-dichlorophenyl)-2-(1H-imidazol-1-yl)ethanone O-(4-methoxybenzoyl) oxime (6l): Off-white powder (0.12 g, 30.0% yield); m.p.: 108 °C; ^{1}H NMR (400 MHz, DMSO-d$_6$): δ=3.87 (s, 3H, CH$_3$) 5.74 (s, 2H, CH$_2$), 6.71 (s, 1H, imidazole H^4), 7.02 (s, 1H, imidazole H^5), 7.11 (d, J = 9.2 Hz, 2H, 4-methoxybenzoyl H^{3,5}), 7.43 (dd, J_1 = 8.4 Hz, J_2 = 2 Hz, 1H, 2,4-dichlorophenyl H^5), 7.48 (d, J = 8.4 Hz, 1H, 2,4-dichlorophenyl H^6), 7.57 (s, 1H, imidazole H^2), 7.64 (d, J = 2 Hz, 1H, 2,4-dichlorophenyl H^3), 8.12 (d, J = 9.2 Hz, 2H, 4-methoxybenzoyl H^{2,6}); ^{13}C NMR (100 MHz, DMSO-d$_6$): δ=44.89 (CH$_2$), 55.62 (CH$_3$), 113.74, 114.35, 119.60, 120.21, 127.23, 128.33, 128.80, 129.74, 131.26, 131.89, 132.12, 132.85, 135.32, 138.15, 161.88, 162.83 (CNO), 163.82 (CO); MS (ESI+) m/z: 406 [M+2+H]$^+$, 404 [M+H]$^+$, 69 (100%); Anal. calcd. for C$_{19}$H$_{15}$Cl$_2$N$_3$O$_3$: C 56.45, H 3.74, N 10.39, found: C 56.09, H 3.85, N 10.19.

1-(2,4-dichlorophenyl)-2-(1H-imidazol-1-yl)ethanone O-(3-phenylprop-2-enoyl) oxime (6m): Off-white powder (0.16 g, 40.0% yield); m.p.: 110.5-2 °C; ^{1}H NMR (400 MHz, DMSO-d$_6$): δ=5.63 (s, 2H, CH$_2$), 6.71 (s, 1H, imidazole H^4), 6.87 (d, J_{AX} = 16.4 Hz, 1H, COCH), 7.02 (s, 1H, imidazole H^5), 7.44-7.47 (m, 5H, 3-phenylprop-2-enoyl H$^{3'-5'}$, 2,4-dichlorophenyl H^{5,6}), 7.56 (s, 1H, imidazole H^2), 7.65 (d, J = 2 Hz, 1H, 2,4-dichlorophenyl H^3), 7.78-7.81 (m, 2H, 3-phenylprop-2-enoyl H$^{2',6'}$), 7.91 (d, J_{XA} = 16.4 Hz, 1H, CHC$_6$H$_5$); ^{13}C NMR (100 MHz, DMSO-d$_6$): δ=44.64 (CH$_2$), 115.24 (imidazole C^5), 120.13 (COCH), 127.27, 128.59 (3C), 128.86, 128.98 (2C), 129.82, 130.98, 132.10, 132.86, 133.86, 135.35, 138.20, 146.69 (CHC$_6$H$_5$), 162.29 (CNO), 162.87 (CO); MS (ESI+) m/z: 422 [M+Na]$^+$ (100%), 402 [M+2+H]$^+$, 400 [M+H]$^+$; Anal. calcd. for C$_{20}$H$_{15}$Cl$_2$N$_3$O$_2$: C 60.02, H 3.78, N 10.50, found: C 59.88, H 3.79, N 10.65.

1-(2,4-dichlorophenyl)-2-(1H-imidazol-1-yl)ethanone O-(4-methylbenzoyl) oxime (6n): Pale yellow powder (0.16 g, 40.5% yield); m.p.: 122 °C; ^{1}H NMR (400 MHz, DMSO-d$_6$): δ=2.43 (s, 3H, CH$_3$), 5.76 (s, 2H, CH$_2$), 6.70 (s, 1H, imidazole H^4), 7.02 (s, 1H, imidazole H^5), 7.41-7.51 (m, 4H, 2,4-dichlorophenyl H^{5,6}, 4-methylbenzoyl H^{3,5}), 7.56 (s, 1H, imidazole H^2), 7.66 (d, J = 2 Hz, 1H, 2,4-dichlorophenyl H^3), 8.06 (d, J = 8.4 Hz, 2H, 4-methylbenzoyl H^{2,6}); MS (ESI+) m/z: 392 [M+4+H]$^+$, 391 [M+4]$^+$, 389 [M+2]$^+$ (100%); Anal. calcd. for C$_{19}$H$_{15}$Cl$_2$N$_3$O$_2$.1/3H$_2$O: C 57.88, H 4.01, N 10.66, found: C 58.06, H 3.92, N 10.74.

1-(2,4-dichlorophenyl)-2-(1H-imidazol-1-yl)ethanone O-(4-isopropylbenzoyl) oxime hydrochloride (6o): Off-white powder (0.16 g, 34.6% yield); m.p.: 113-6 °C; ^{1}H NMR (400 MHz, DMSO-d$_6$): δ=1.24 (d, J = 7.2 Hz, 6H, CH$_3$), 3.00-3.03 (m, 1H, CH(CH$_3$)$_2$), 6.07 (s, 2H, CH$_2$), 7.49 (d, J = 8.4 Hz, 2H, 4-isopropylbenzoyl H^{3,5}), 7.51 (s, 1H, imidazole H^4), 7.54 (dd, J_1 =

8.4 Hz, J_2 = 2 Hz, 1H, 2,4-dichlorophenyl H[5]), 7.60 (s, 1H, imidazole H[5]), 7.66 (d, J = 8.8 Hz, 1H, 2,4-dichlorophenyl H[6]), 7.72 (d, J = 2 Hz, 1H, 2,4-dichlorophenyl H[3]), 8.08 (d, J = 8.4 Hz, 2H, 4-isopropylbenzoyl H[2,6]), 9.17 (s, 1H, imidazole H[5]); MS (ESI+) m/z: 420 [M+4+H]$^+$, 419 [M+4]$^+$, 417 [M+2]$^+$ (100%); Anal. calcd. for $C_{21}H_{20}Cl_3N_3O_2 \cdot H_2O$: C 53.58, H 4.71, N 8.93, found: C 53.16, H 4.78, N 8.87.

1-(2,4-dichlorophenyl)-2-(1H-imidazol-1-yl)ethanone O-(cyclohexanecarbonyl) oxime (6p): White powder (0.14 g, 38.0% yield); m.p.: 101-3 °C; ^{1}H NMR (400 MHz, DMSO-d_6): δ=1.22-2.65 (m, 11H, cyclohexane), 5.53 (s, 1H, CH_2N), 6.70 (s, 1H, imidazole H[4]), 6.99 (s, 1H, imidazole H[5]), 7.43 (m, 2H, 2,4-dichlorophenyl H[5,6]), 7.53 (s, 1H, imidazole H[2]), 7.64 (s, 1H, 2,4-dichlorophenyl H[3]); ^{13}C NMR (100 MHz, DMSO-d_6): δ=24.77 (2C, cyclohexane C[3,5]), 25.17 (cyclohexane C[4]), 28.41 (2C, cyclohexane C[2,6]), 41.02 (cyclohexane C[1]), 44.61 (CH_2N), 120.14, 127.25, 128.39, 128.83, 129.78, 132.06, 132.79, 135.30, 138.16, 162.37 (CNO), 171.29 (CO); MS (ESI+) m/z: 384 [M+4+H]$^+$, 383 [M+4]$^+$, 380 [M+2]$^+$ (100%); Anal. calcd. for $C_{18}H_{19}Cl_2N_3O_2 \cdot 1/2H_2O$: C 55.54, H 5.18, N 10.79, found: C 55.83, H 5.61, N 10.69.

1-(2,4-dichlorophenyl)-2-(1H-imidazol-1-yl)ethanone O-(benzoyl) oxime (6q): White powder (0.16 g, 42.0% yield); m.p.: 117-9 °C; ^{1}H NMR (400 MHz, DMSO-d_6): δ=5.78 (s, 2H, CH_2), 6.71 (s, 1H, imidazole H[4]), 7.04 (s, 1H, imidazole H[5]), 7.46 (dd, J_1 = 8.4 Hz, J_2 = 2 Hz, 1H, 2,4-dichlorophenyl H[5]), 7.51 (d, J = 8.4 Hz, 1H, 2,4-dichlorophenyl H[6]), 7.57 (s, 1H, imidazole H[2]), 7.61-7.65 (m, 2H, benzoyl H[3,5]), 7.67 (d, J = 2 Hz, 1H, 2,4-dichlorophenyl H[3]), 7.75-7.79 (m, 1H, benzoyl H[4]), 8.17-8.20 (m, 2H, benzoyl H[2,6]); ^{13}C NMR (100 MHz, DMSO-d_6): δ=44.91 (CH_2), 120.19, 127.27, 127.68, 128.55, 128.83, 129.06 (2C), 129.61, 129.67 (2C), 132.11, 132.84, 134.21, 135.39, 138.23, 162.26 (CNO), 163.57 (CO); MS (ESI+) m/z: 396 [M+Na]$^+$ (100%), 376 [M+2+H]$^+$, 374 [M+H]$^+$; Anal. calcd. for $C_{18}H_{13}Cl_2N_3O_2 \cdot 1/2H_2O$: C 56.41, H 3.68, N 10.97, found: C 56.55, H 3.69, N 11.31.

1-(2,4-dichlorophenyl)-2-(1H-imidazol-1-yl)ethanone O-(quinoline-2-carbonyl) oxime hydrochloride (6r): White powder (0.16 g, 42.0% yield); m.p.: 117-9 °C; ^{1}H NMR (400 MHz, DMSO-d_6): δ=6.08 (s, 2H, CH_2), 7.60-7.62 (m, 2H, 2,4-dichlorophenyl H[5], quinoline H[6]), 7.74 (d, J = 8.4 Hz, 1H, 2,4-dichlorophenyl H[6]), 7.80-7.86 (m, 3H, imidazole H[4,5], 2,4-dichlorophenyl H[3]), 7.95-7.99 (m, 1H, quinoline H[7]), 8.19 (d, J = 7.6 Hz, 1H, quinoline H[8]), 8.29 (d, J = 8.8 Hz, 1H, quinoline H[5]), 8.33 (d, J = 8.4 Hz, 1H, quinoline H[3]), 8.73 (d, J = 8.4 Hz, 1H, quinoline H[4]), 9.38 (s, 1H, imidazole H[2]); ^{13}C NMR (100 MHz, DMSO-d_6): δ=47.19 (CH_2), 120.09, 121.19,

123.03, 127.88, 128.18, 129.06, 129.25, 129.27, 129.32, 129.90, 131.05, 132.67, 132.80, 136.23, 136.92, 138.22, 146.02, 146.90, 161.01 (CNO), 161.66 (CO); MS (ESI+) m/z: 428 $[M+4]^{+}$, 426 $[M+2]^{+}$ (100%), 425 $[M+H]^{+}$; Anal. calcd. for $C_{21}H_{15}Cl_3N_4O_2$: C 54.63, H 3.27, N 12.13, found: C 54.13, H 3.48, N 12.09.

4.2.2. X ray crystallography studies

A Rigaku R-Axis Rapid II DW Micro Max 007DW XG and VariMax DW optics single crystal X-ray diffractometer system with curved imaging plate detector was used to collect the reflection data of **4** and **5o** at 293 K. The data collection, cell refinement and data reduction were performed by CrystalClear-SM Expert 2.0 r16 program (*CrystalClear* 2014. Rigaku Corporation, Tokyo, Japan). The crystal structures were solved by direct methods using SIR2011 [52] and, refinements were performed with SHELXL2014 [53] for both structures. Except the hydrogen atom (H5) of the chiral atom C5 of **5o**, all the H atoms were positioned at their ideal locations and refined using the AFIX commends according to their C atoms attached. The H5 of C5 of **5o** was positioned from difference Fourier map. All non-hydrogen atoms of the two structures were treated anistropically. The geometric calculations were performed using the program PLATON [54].

Crystals of **4** was crystallized under a monoclinic space group P2/c and its unit cell constants were $a = 9.7881(2)$ Å, $b = 8.73300(10)$ Å, $c = 14.3658(10)$ Å, $\beta = 93.221(7)°$, $V = 1226.04(9)$ Å^3, and $Z = 4$ (at 293 K). The supplementary information in the CIF form is available from Cambridge Crystallographic Database Centre, No. CCDC 1901941. Crystals of **5o** belongs to the monoclinic space group C2/c. Its unit cell constants were found $a = 32.9738(3)$ Å, $b = 9.9105(4)$ Å, $c = 12.9770(7)$ Å, $\beta = 98.263(6)°$, $V = 4196.7(3)$ Å^3, and $Z = 8$ (at 293 K). The supplementary information in the CIF form is available from Cambridge Crystallographic Database Centre, No. CCDC 1901940. The details for the crystal data and the structure refinements can be found in Table S2 of Supporting Information.

4.3. Biological activity studies

4.3.1. Antifungal susceptibility tests

Microdilution assay: The MIC values of the compounds against certain *Candida* spp. were determined using the broth microdilution method according to the Clinical and Laboratory Standards Institute (CLSI) reference documents [55]. Three commercial *Candida* strains (*C.*

albicans ATCC 90028, *C. krusei* ATCC 6258, and *C. parapsilosis* ATCC 90018) that are azole-susceptible and one azole-resistant *C. tropicalis* isolate were included in this test and fluconazole was used as positive control. Before the test, the fungi samples stored at −80 °C in glycerol were thawed and subcultured twice onto Sabouraud dextrose agar. RPMI 1640 broth (ICN-Flow, Aurora, OH, USA, with glutamine, without bicarbonate and with pH indicator) buffered to pH 7.0 with 3-*N*-morpholinopropanesulfonic acid (Sigma, USA) was used as medium and the inoculum densities were prepared from 24-hour subcultures. The final test concentrations of fungi were 0.5 to 2.5 × 10^3 cfu/ml. Fluconazole was dissolved in sterile deionized distilled water (64–0.0625 µg/ml) and the compounds were solvated in DMSO (Sigma, USA). Final twofold concentrations of the compounds were prepared in the wells of the microtiter plates, between 1024 and 0.125 µg/ml. The plates were incubated at 35 °C for 48 hours. MIC values were determined as the lowest concentration of test compound that inhibited visual growth completely.

Antibiofilm assay: *C. albicans* SC5314 biofilms were grown in the Calgary Biofilm Device (commercially available as the MBEC Assay™ for Physiology & Genetics, P & G, Innovotech Inc., Edmonton, Alberta, Canada) according to the MBEC™ assay protocol, a standard ASTM method, as supplied by the manufacturer. Aliquots of 150 µl final inoculum suspension (106 cfu/ml) were transferred to each test well and the 96-peg MBEC assay plate lids were placed into the microtiter plates. The plates were incubated for 24 hours at 37 °C to form mature biofilms. After 24 hours, the peg lids of the MBEC assay plates were rinsed three times with 100 µl 0.9% physiological saline (PS), then transferred to a "challenge" plate. Finally, 200 µl serial twofold dilutions of each compound were subsequently added to each well and incubated for 24 hours at 35 °C. The concentrations of the compounds ranged between 512-0.5 µg/ml in columns 1-11, respectively. Positive growth control (amphotericin B) and sterility control were included in each plate. After 24-hour treatment of the biofilms, the peg lids were rinsed three times in 0.9% PS and transferred to a "recovery" plate, each well of which contained RPMI 1640 supplemented with 2% glucose. The plates were sonicated for five minutes to remove the biofilms into recovery media, the recovery plates were incubated overnight and optical densities of the wells were measured at 550 nm by spectrophotometer. The plates were also visually checked after 24 hours for turbidity and clear wells were taken as evidence of biofilm eradication. The MBEC values were determined

upon identification of the lowest antibiotic concentration that prevents regrowth of *C. albicans* from the treated biofilm and the MBIC values, of the minimum concentration that prevents the initial formation of biofilm by visual inspection of the wells for turbidity.

4.3.2. Cytotoxicity assay

The cytotoxic effects of the compounds were evaluated *in vitro* according to the 3-(4,5-dimethylthiazol-2-yl)-2,5-diphenyltetrazolium bromide (MTT) reduction assay [56]. The assay was performed on human monocytic cell line (U937) obtained from Hacettepe University, Basic Oncology Department. The cells (4 x 10^3 cells/well) were seeded into 96-well plates in 50 μl of RPMI-1640 with 10% fetal bovine serum, L-glutamine (2 mM), penicillin (50 U/ml), and streptomycin (50 μg/ml). The compounds were dissolved in cell culture medium with the help of DMSO (maximum DMSO concentration was 0.32%, v/v) and 50 μl of these solutions were added to wells to obtain final compound concentrations ranging from 0.125-32 μg/ml. The cells were exposed to eight concentrations of compounds and each concentration and control were analyzed in triplicate. The cells and compounds were incubated at 37 °C in 5% CO_2 for 24 and 48 h, then 20 μl MTT solution (5 mg/ml) was added to each well and the plates were then incubated at 37 °C in 5% CO_2 for an additional 4 h. Later, 80 μl 23% sodium dodecyl sulfate (SDS) solution in 45% DMF (pH 4.7) was added to the wells to dissolve formazan crystals, and the plates were incubated overnight at 37 °C in 5% CO_2. Absorbance of wells was measured at 570 nm using a microplate reader (Molecular Devices, USA) and the cell viability of each treatment was calculated using untreated cells as control.

References

[1] S. Silva, M. Negri, M. Henriques, R. Oliveira, D.W. Williams, J. Azeredo, Candida glabrata, Candida parapsilosis and Candida tropicalis: biology, epidemiology, pathogenicity and antifungal resistance, FEMS Microbiol. Rev. 36 (2012) 288-305. https://doi.org/10.1111/j.1574-6976.2011.00278.x

[2] J.E. Nett, Special Issue: Candida and Candidiasis, J. Fungi (Basel) 4 (2018) 74. https://doi.org/10.3390/jof4030074

[3]   L. Krishnasamy, S. Krishnakumar, G. Kumaramanickavel, C. Saikumar, Molecular Mechanisms of Antifungal Drug Resistance in Candida Species, J. Clin. Diagn. Res. 12 (2018) De1-De6. https://doi.org/10.1016/j.jgar.2014.09.002

[4]   G. Garcia-Effron, D.P. Kontoyiannis, R.E. Lewis, D.S. Perlin, Caspofungin-resistant Candida tropicalis strains causing breakthrough fungemia in patients at high risk for hematologic malignancies, Antimicrob. Agents Chemother. 52 (2008) 4181-4183. https://doi.org/10.1128/AAC.00802-08

[5]   H. Dermoumi, In vitro susceptibility of yeast isolates from the blood to fluconazole and amphotericin B, Chemotherapy 38 (1992) 112-117. http://dx.doi.org/10.1155/2013/236903

[6]   R.M. Donlan, Biofilms: microbial life on surfaces, Emerg. Infect. Dis. 8 (2002) 881-890. https://doi.org/10.3201/eid0809.020063

[7]   M.A. Jabra-Rizk, W.A. Falkler, T.F. Meiller, Fungal biofilms and drug resistance, Emerg. Infect. Dis. 10 (2004) 14-19. https://dx.doi.org/10.3201/eid1001.030119

[8]   N.M. Martinez-Rossi, T.A. Bitencourt, N.T.A. Peres, E.A.S. Lang, E.V. Gomes, N.R. Quaresemin, M.P. Martins, L. Lopes, A. Rossi, Dermatophyte Resistance to Antifungal Drugs: Mechanisms and Prospectus, Front. Microbiol. 9 (2018) 1108. https://doi.org/10.3389/fmicb.2018.01108

[9]   J.R. Graybill, Future directions of antifungal chemotherapy, Clin. Infect. Dis. 14 Suppl 1 (1992) S170-181. https://doi.org/10.1093/clinids/14.Supplement_1.S170

[10]   H. Madhosingh, F.S. Southwick, Infectious Diseases, in: M.P. Harward (Ed.) Medical Secrets, Elsevier Mosby, Philadelphia, 2012, pp. 344-375.

[11]   I.S. Dogan, S. Sarac, S. Sari, D. Kart, S.E. Gokhan, I. Vural, S. Dalkara, New azole derivatives showing antimicrobial effects and their mechanism of antifungal activity by molecular modeling studies, Eur. J. Med. Chem. 130 (2017) 124-138. https://doi.org/10.1016/j.ejmech.2017.02.035

[12]   B. Sun, W. Huang, M. Liu, Evaluation of the combination mode of azoles antifungal inhibitors with CACYP51 and the influence of Site-directed mutation, J. Mol. Graph. Model. 73 (2017) 157-165. https://doi.org/10.1016/j.jmgm.2017.02.009

[13] B. Sun, H. Zhang, M. Liu, Z. Hou, X. Liu, Structure-based virtual screening and ADME/T-based prediction analysis for the discovery of novel antifungal CYP51 inhibitors, MedChemComm 9 (2018) 1178-1187. https://doi.org/10.1039/c8md00230d

[14] N. Thamban Chandrika, S.K. Shrestha, H.X. Ngo, O.V. Tsodikov, K.C. Howard, S. Garneau-Tsodikova, Alkylated Piperazines and Piperazine-Azole Hybrids as Antifungal Agents, J. Med. Chem. 61 (2018) 158-173. https://doi.org/10.1021/acs.jmedchem.7b01138

[15] J. Wu, T. Ni, X. Chai, T. Wang, H. Wang, J. Chen, Y. Jin, D. Zhang, S. Yu, Y. Jiang, Molecular docking, design, synthesis and antifungal activity study of novel triazole derivatives, Eur. J. Med. Chem. 143 (2018) 1840-1846. https://doi.org/10.1016/j.ejmech.2017.10.081

[16] C.M. Yates, E.P. Garvey, S.R. Shaver, R.J. Schotzinger, W.J. Hoekstra, Design and optimization of highly-selective, broad spectrum fungal CYP51 inhibitors, Bioorg. Med. Chem. Lett. 27 (2017) 3243-3248. https://doi.org/10.1016/j.bmcl.2017.06.037

[17] V.W. Rabelo, T.F. Santos, L. Terra, M.V. Santana, H.C. Castro, C.R. Rodrigues, P.A. Abreu, Targeting CYP51 for drug design by the contributions of molecular modeling, Fundam. Clin. Pharmacol. 31 (2017) 37-53. https://doi.org/10.1111/fcp.12230

[18] C.A. Lipinski, F. Lombardo, B.W. Dominy, P.J. Feeney, Experimental and computational approaches to estimate solubility and permeability in drug discovery and development settings, Adv. Drug Deliv. Rev. 46 (2001) 3-26. https://doi.org/10.1016/S0169-409X(96)00423-1

[19] J. Kelder, P.D. Grootenhuis, D.M. Bayada, L.P. Delbressine, J.P. Ploemen, Polar molecular surface as a dominating determinant for oral absorption and brain penetration of drugs, Pharm. Res. 16 (1999) 1514-1519. https://doi.org/10.1023/A:1015040217741

[20] D.F. Veber, S.R. Johnson, H.Y. Cheng, B.R. Smith, K.W. Ward, K.D. Kopple, Molecular properties that influence the oral bioavailability of drug candidates, J. Med. Chem. 45 (2002) 2615-2623. https://doi.org/10.1021/jm020017n

[21] B.C. Monk, T.M. Tomasiak, M.V. Keniya, F.U. Huschmann, J.D. Tyndall, J.D. O'Connell, 3rd, R.D. Cannon, J.G. McDonald, A. Rodriguez, J.S. Finer-Moore, R.M. Stroud,

Architecture of a single membrane spanning cytochrome P450 suggests constraints that orient the catalytic domain relative to a bilayer, Proc. Natl. Acad. Sci. U. S. A. 111 (2014) 3865-3870. https://doi.org/10.1073/pnas.1324245111

[22]   A.A. Sagatova, M.V. Keniya, R.K. Wilson, B.C. Monk, J.D. Tyndall, Structural Insights into Binding of the Antifungal Drug Fluconazole to Saccharomyces cerevisiae Lanosterol 14alpha-Demethylase, Antimicrob. Agents Chemother. 59 (2015) 4982-4989. https://do,.org/10.1128/AAC.00925-15

[23]   M.A. Correia, P.R.O.d. Montellano, Inhibition of Cytochrome P450 Enzymes, in: P.R.O.d. Montellano (Ed.) Cytochrome P450: Structure, Mechanism, and Biochemistry, Kluwer Academic-Plenum Publishing, New York, 2005.

[24]   G.M. Morris, R. Huey, W. Lindstrom, M.F. Sanner, R.K. Belew, D.S. Goodsell, A.J. Olson, AutoDock4 and AutoDockTools4: Automated docking with selective receptor flexibility, J. Comput. Chem. 30 (2009) 2785-2791. https://doi.org/10.1002/jcc.21256

[25]   R.A. Friesner, J.L. Banks, R.B. Murphy, T.A. Halgren, J.J. Klicic, D.T. Mainz, M.P. Repasky, E.H. Knoll, M. Shelley, J.K. Perry, D.E. Shaw, P. Francis, P.S. Shenkin, Glide: a new approach for rapid, accurate docking and scoring. 1. Method and assessment of docking accuracy, J. Med. Chem. 47 (2004) 1739-1749. https://doi.org/10.1021/jm0306430

[26]   R.A. Friesner, R.B. Murphy, M.P. Repasky, L.L. Frye, J.R. Greenwood, T.A. Halgren, P.C. Sanschagrin, D.T. Mainz, Extra precision glide: docking and scoring incorporating a model of hydrophobic enclosure for protein-ligand complexes, J. Med. Chem. 49 (2006) 6177-6196. https://doi.org/10.1021/jm051256o

[27]   T.A. Halgren, R.B. Murphy, R.A. Friesner, H.S. Beard, L.L. Frye, W.T. Pollard, J.L. Banks, Glide: a new approach for rapid, accurate docking and scoring. 2. Enrichment factors in database screening, J. Med. Chem, 47 (2004) 1750-1759. https://doi.org/10.1021/jm030644s

[28]   R. Wang, S. Wang, How does consensus scoring work for virtual library screening? An idealized computer experiment, J. Chem. Inf. Comput. Sci. 41 (2001) 1422-1426. https://doi.org/10.1021/ci010025x

[29] M. Stahl, M. Rarey, Detailed analysis of scoring functions for virtual screening, J. Med. Chem. 44 (2001) 1035-1042. https://doi.org/10.1021/jm0003992

[30] K.A. Walker, D.R. Hirschfeld, M. Marx, Antimycotic imidazoles. 2. Synthesis and antifungal properties of esters of 1-[2-hydroxy(mercapto)-2-phenylethyl]-1H-imidazoles, J. Med. Chem. 21 (1978) 1335-1338.

[31] D. De Vita, G. Simonetti, F. Pandolfi, R. Costi, R. Di Santo, F.D. D'Auria, L. Scipione, Exploring the anti-biofilm activity of cinnamic acid derivatives in Candida albicans, Bioorg. Med. Chem. Lett. 26 (2016) 5931-5935. https://doi.org/10.1016/j.bmcl.2016.10.091

[32] L.J. Farrugia, ORTEP-3 for Windows - a version of ORTEP-III with a Graphical User Interface (GUI), J. Appl. Crystallogr. 30 (1997) 565. https://doi.org/10.1107/S0021889897003117

[33] S. Sari, S. Dalkara, F.B. Kaynak, J. Reynisson, S. Sarac, A. Karakurt, New Anti-Seizure (Arylalkyl)azole Derivatives: Synthesis, In Vivo and In Silico Studies, Arch. Pharm. 350 (2017) e201700043. https://doi.org/10.1002/ardp.201700043

[34] S. Sari, A. Karakurt, H. Uslu, F.B. Kaynak, U. Calis, S. Dalkara, New (arylalkyl)azole derivatives showing anticonvulsant effects could have VGSC and/or GABAAR affinity according to molecular modeling studies, Eur. J. Med. Chem. 124 (2016) 407-416. https://doi.org/10.1016/j.ejmech.2016.08.032

[35] S. Sari, F.B. Kaynak, S. Dalkara, Synthesis and anticonvulsant screening of 1,2,4-triazole derivatives, Pharmacol. Rep. (2018) 1116-1123. https://doi.org/10.1016/j.pharep.2018.06.007

[36] F. Morio, C. Loge, B. Besse, C. Hennequin, P. Le Pape, Screening for amino acid substitutions in the Candida albicans Erg11 protein of azole-susceptible and azole-resistant clinical isolates: new substitutions and a review of the literature, Diagn. Microbiol. Infect. Dis. 66 (2010) 373-384. https://doi.org/10.1016/j.diagmicrobio.2009.11.006

[37] J.L. Banks, H.S. Beard, Y. Cao, A.E. Cho, W. Damm, R. Farid, A.K. Felts, T.A. Halgren, D.T. Mainz, J.R. Maple, R. Murphy, D.M. Philipp, M.P. Repasky, L.Y. Zhang, B.J. Berne, R.A.

Friesner, E. Gallicchio, R.M. Levy, Integrated Modeling Program, Applied Chemical Theory (IMPACT), J Comput Chem, 26 (2005) 1752-1780.

[38] N. Eswar, B. Webb, M.A. Marti-Renom, M.S. Madhusudhan, D. Eramian, M.Y. Shen, U. Pieper, A. Sali, Comparative protein structure modeling using Modeller, Curr. Protoc. Bioinformatics 15 (2006) 5.6.1-5.6.30. https://doi.org/10.1002/0471250953.bi0506s15

[39] W. Humphrey, A. Dalke, K. Schulten, VMD: visual molecular dynamics, J. Mol. Graph. 14 (1996) 33-38. https://doi.org/10.1016/0263-7855(96)00018-5

[40] R.B. Best, X. Zhu, J. Shim, P.E. Lopes, J. Mittal, M. Feig, A.D. Mackerell, Jr., Optimization of the additive CHARMM all-atom protein force field targeting improved sampling of the backbone phi, psi and side-chain chi(1) and chi(2) dihedral angles, J. Chem. Theory Comput. 8 (2012) 3257-3273. https://dx.doi.org/10.1021/ct300400x

[41] W.L. Jorgensen, J. Chandrasekhar, J.D. Madura, R.W. Impey, M.L. Klein, Comparison of simple potential functions for simulating liquid water, J. Chem. Phys. 79 (1983) 926-935.

[42] A.D. MacKerell, D. Bashford, M. Bellott, R.L. Dunbrack, J.D. Evanseck, M.J. Field, S. Fischer, J. Gao, H. Guo, S. Ha, D. Joseph-McCarthy, L. Kuchnir, K. Kuczera, F.T. Lau, C. Mattos, S. Michnick, T. Ngo, D.T. Nguyen, B. Prodhom, W.E. Reiher, B. Roux, M. Schlenkrich, J.C. Smith, R. Stote, J. Straub, M. Watanabe, J. Wiorkiewicz-Kuczera, D. Yin, M. Karplus, All-atom empirical potential for molecular modeling and dynamics studies of proteins, J. Phys. Chem. B 102 (1998) 3586-3616. https://doi.org/10.1021/jp973084f

[43] A.D. MacKerell, Jr., M. Feig, C.L. Brooks, 3rd, Improved treatment of the protein backbone in empirical force fields, J. Am. Chem. Soc. 126 (2004) 698-699. https://doi.org/10.1021/ja036959e

[44] K. Vanommeslaeghe, E. Hatcher, C. Acharya, S. Kundu, S. Zhong, J. Shim, E. Darian, O. Guvench, P. Lopes, I. Vorobyov, A.D. Mackerell, Jr., CHARMM general force field: A force field for drug-like molecules compatible with the CHARMM all-atom additive biological force fields, J. Comput. Chem. 31 (2010) 671-690. https://doi.org/10.1002/jcc.21367

[45] W. Yu, X. He, K. Vanommeslaeghe, A.D. MacKerell, Jr., Extension of the CHARMM General Force Field to sulfonyl-containing compounds and its utility in biomolecular simulations, J. Comput. Chem. 33 (2012) 2451-2468. https://doi.org/10.1002/jcc.23067

[46] T. Darden, D. York, L. Pedersen, Particle mesh Ewald: An N·log(N) method for Ewald sums in large systems, J. Chem. Phys. 98 (1993) 10089-10092. https://doi.org/10.1063/1.464397

[47] J.C. Phillips, R. Braun, W. Wang, J. Gumbart, E. Tajkhorshid, E. Villa, C. Chipot, R.D. Skeel, L. Kale, K. Schulten, Scalable molecular dynamics with NAMD, J. Comput. Chem. 26 (2005) 1781-1802. https://doi.org/10.1002/jcc.20289

[48] J.P. Ryckaert, G. Ciccotti, H.J.C. Berendsen, Numerical-Integration of Cartesian Equations of Motion of a System with Constraints - Molecular-Dynamics of N-Alkanes, J. Comput. Phys. 23 (1977) 327-341.

[49] H. Baji, M. Flammang, T. Kimny, F. Gasquez, P.L. Compagnon, A. Delcourt, Synthesis and antifungal activity of novel (1-aryl-2-heterocyclyl)ethylideneaminooxymethyl-substituted dioxolanes, Eur. J. Med. Chem. 30 (1995) 617-626. https://doi.org/10.1016/0223-5234(96)88277-8

[50] E.F. Godefroi, J. Heeres, J. Van Cutsem, P.A. Janssen, The preparation and antimycotic properties of derivatives of 1-phenethylimidazole, J. Med. Chem. 12 (1969) 784-791.

[51] B. Neises, W. Steglich, Simple Method for the Esterification of Carboxylic Acids, Angew. Chem. Int. Ed. 17 (1978) 522-524.

[52] M.C. Burla, R. Caliandro, M. Camalli, B. Carrozzini, G.L. Cascarano, C. Giacovazzo, M. Mallamo, A. Mazzone, G. Polidori, R. Spagna, SIR2011: a new package for crystal structure determination and refinement, J. Appl. Crystallogr. 45 (2012) 357-361. https://doi.org/10.1107/S0021889812001124

[53] G.M. Sheldrick, Crystal structure refinement with SHELXL, Acta Crystallogr. C 71 (2015) 3-8. https://doi.org/10.1107/S2053229614024218

[54] A.L. Spek, Structure validation in chemical crystallography, Acta Crystallogr. D 65 (2009) 148-155. https://doi.org/10.1107/S090744490804362X

[55] CLSI, Refence Method for Broth Dilution Antifungal Susceptibility Testing of Yeasts, Wayne, 2008.

[56] T. Mosmann, Rapid colorimetric assay for cellular growth and survival: application to proliferation and cytotoxicity assays, J. Immunol. Methods 65 (1983) 55-63. https://doi.org/10.1016/0022-1759(83)90303-4

A

B

C

D
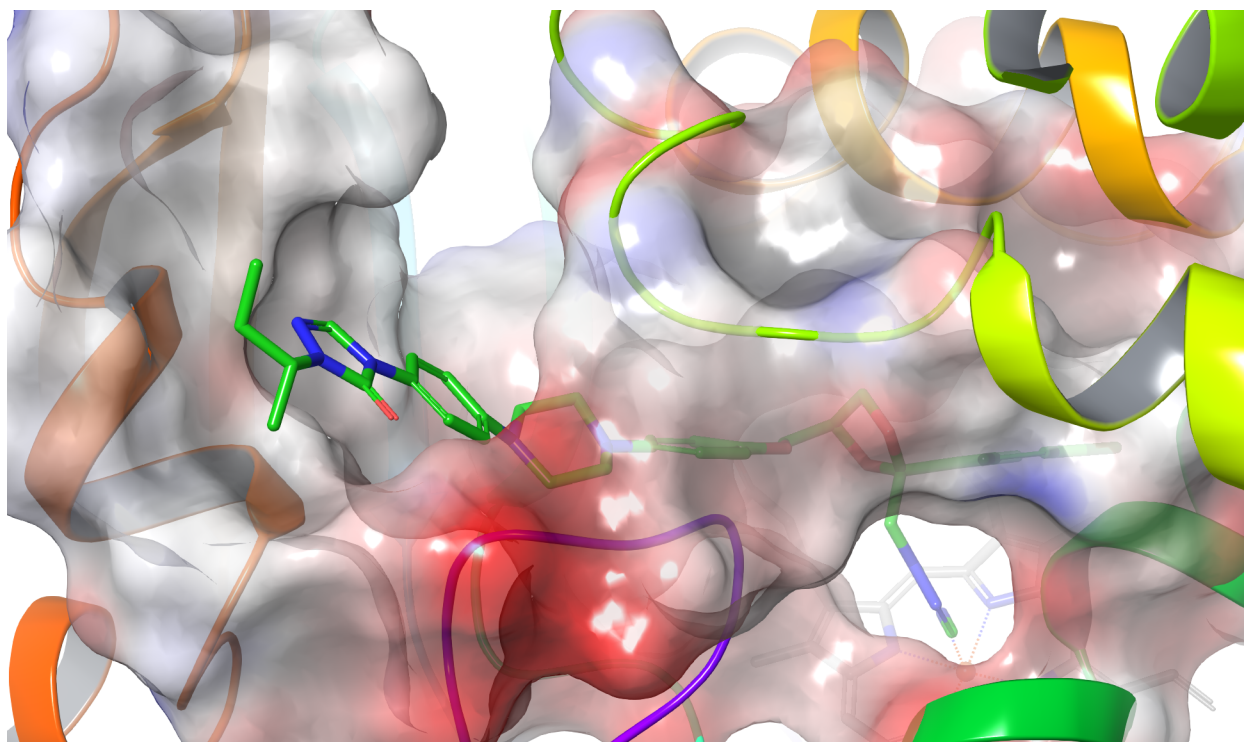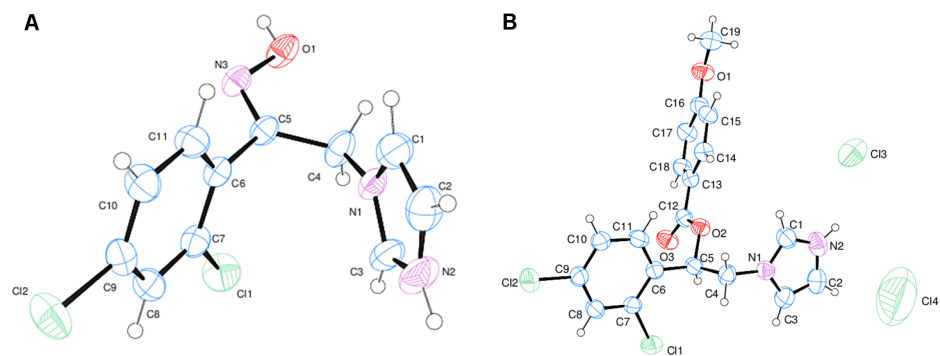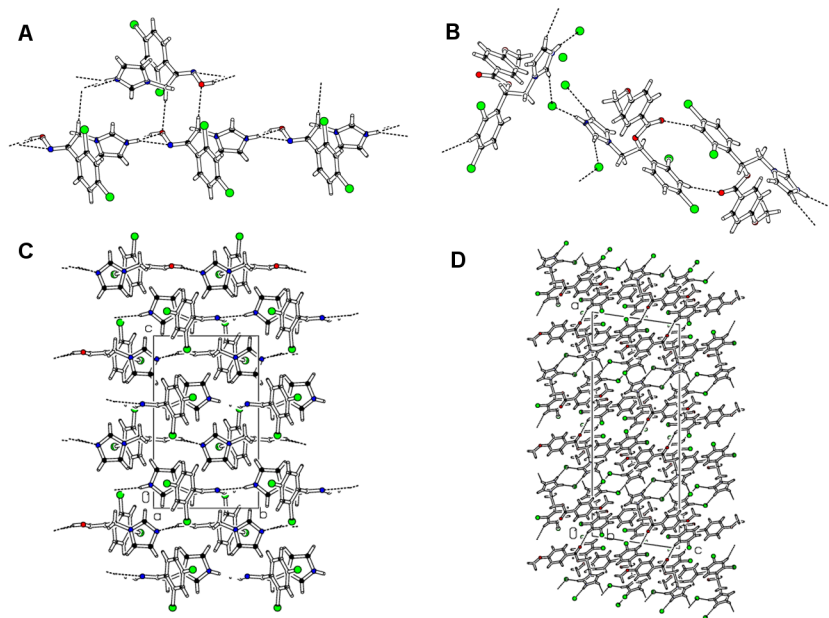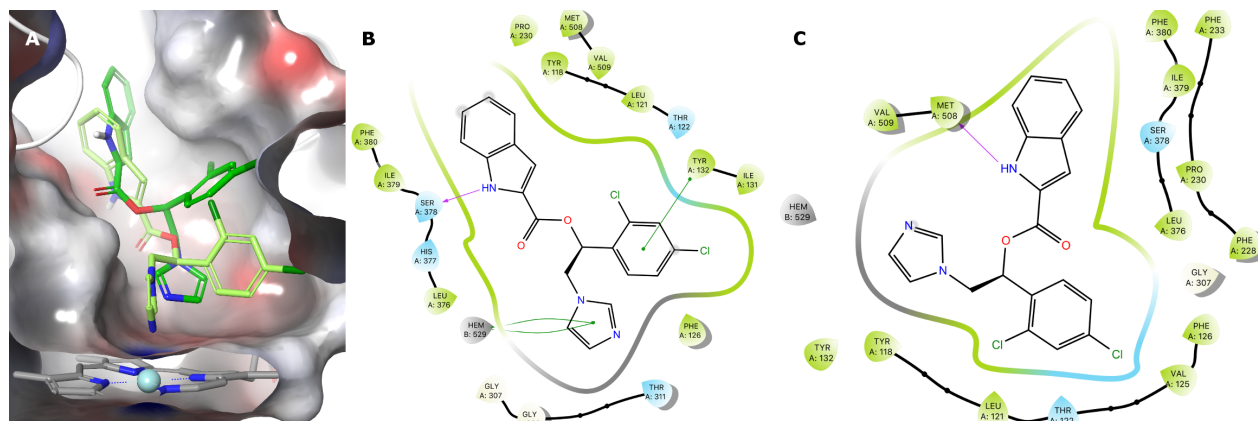
- Using consensus scoring for virtual screening 38 azole derivatives were identified.

- The derivatives were synthesized and tested for antifungal activity.

- Many hits with potent activity against *Candida* spp. were obtained.

- Some were active against resistant *C. tropicalis* isolate and *C. albicans* biofilms.

- MD simulations were run to provide insights into mechanism of action.